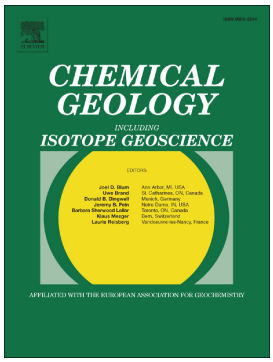

Carbon-sulfur signals of methane versus crude oil diagenetic decomposition and U-Th age relationships for authigenic carbonates from asphalt seeps, southern Gulf of Mexico

Sajjad A. Akam, Timothy W. Lyons, Richard B. Coffin, David McGee, Thomas H. Naehr, Steven M. Bates, Clay Clarkson, Brandi Kiel Reese

PII: S0009-2541(21)00338-7

DOI: https://doi.org/10.1016/j.chemgeo.2021.120395

Reference: CHEMGE 120395

To appear in: *Chemical Geology*

Received date: 16 August 2020

Revised date: 9 June 2021

Accepted date: 11 June 2021

Please cite this article as: S.A. Akam, T.W. Lyons, R.B. Coffin, et al., Carbon-sulfur signals of methane versus crude oil diagenetic decomposition and U-Th age relationships for authigenic carbonates from asphalt seeps, southern Gulf of Mexico, *Chemical Geology* (2021), https://doi.org/10.1016/j.chemgeo.2021.120395

Carbon-sulfur signals of methane versus crude oil diagenetic decomposition and U-Th age relationships for authigenic carbonates from asphalt seeps, southern Gulf of Mexico.

Sajjad A. Akam[1,2], Timothy W. Lyons[3], Richard B. Coffin[2], David McGee[4], Thomas H. Naehr[5], Steven M. Bates[3], Clay Clarkson[2], Brandi Kiel Reese[6,7]

[1] Department of Tribal Environmental Science, United Tribes Technical College, Bismarck, North Dakota, United States

[2] Department of Physical and Environmental Sciences, Texas A&M University-Corpus Christi, Corpus Christi, Texas, United States

[3] Department of Earth Sciences, University of California, Riverside, California, United States

[4] Department of Earth and Planetary Sciences, Massachusetts Institute of Technology, Cambridge, Massachusetts, United States

[5] Department of Geological and Environmental Sciences, University of the Pacific, Stockton, California, United States

[6] Dauphin Island Sea Lab, Dauphin Island, Alabama, United States

[7] University of South Alabama, Department of Marine Sciences, Mobile, Alabama, USA

Abstract:

Offshore hydrocarbon accumulations in the Gulf of Mexico (GoM) are often accompanied by natural seepage of oil and gas from subsurface reservoirs into shallow sediments and the water column. This study investigated the temporal patterns and carbon-sulfur (C-S) coupling associated with authigenic carbonate samples recovered from surface sediments of a crude oil seepage site in southern GoM (Chapopote asphalt volcano, Bay of Campeche) using radioactive U-Th dates, and stable C, O, and S isotopes. The results were compared with data from multiple seep sites in the northern GoM where methane seepage is dominant along with non-methane hydrocarbons (ethane , propane, crude oil, etc.). U-Th age-dating of Chapopote seep carbonate samples yielded ages of 13.5 ka to 4.6 ka before present (BP), suggesting that Chapopote asphalt seepage has been ongoing for thousands of years. The results are also consistent with previous studies from the northern GoM that hypothesize that seeps along the GoM continental slope were active during the last deglaciation. $\delta^{13}C_{CaCO3}$ and $\delta^{18}O_{CaCO3}$ values from authigenic carbonates at Chapopote indicated a mixed contribution of methane and non-methane hydrocarbons to the dissolved inorganic carbon (DIC) pool, consistent with previous results. Comparison of $\delta^{13}C_{CaCO3}$ vs. $\delta^{34}S_{CRS}$ (CRS = chromium reducible sulfur) from carbonate samples showed

noticeable differences at the Chapopote seep site (average $\delta^{13}C_{CaCO3}$ -25‰ VDPB, $\delta^{34}S_{CRS}$ -27‰ VCDT) relative to the methane seep-dominated samples from the northern GoM (average $\delta^{13}C_{CaCO3}$ < -40‰ VDPB, $\delta^{34}S_{CRS}$ >0‰ VCDT). Our results point toward distinguishable differences in the paired $\delta^{13}C_{DIC}$ and $\delta^{34}S_{sulfide}$ signatures produced via the diagenetic processes of sulfate-driven anaerobic oxidation of methane versus non-methane hydrocarbons. These results potentially provide an important proxy for identification of such diagenetic processes within the sedimentary records.

Keywords: Hydrocarbon seeps, authigenic carbonates, U-Th dating, Gulf of Mexico, microbial sulfate reduction, anaerobic hydrocarbon oxidation, Carbon-Sulfur cycling

1. Introduction

Tectonic and depositional conditions in the Gulf of Mexico (GoM) provide an ideal setting for the formation of oil and gas as well as its upward migration from subsurface reservoirs to the seafloor and water column (Sassen et al., 1998). Natural hydrocarbon seeps may account for ~47% of all crude oil entering the marine environment (Kvenvolden and Cooper, 2003), with an estimated 160 to 690 thousand barrels of oil entering the Gulf of Mexico annually (Kvenvolden and Harbaugh, 1983; Mitchell et al., 1999; National Research Council, 2003; MacDonald et al., 2015). These seepage sites have a significant impact on geology and biology of the seabed facilitated by microbially-mediated biogeochemical processes (Judd and Hovland, 2009; Hovland et al., 2012; Coffin et al., 2015; Chakraborty et al., 2020).

GoM seeps are characterized by significant quantities of authigenic minerals formed by the activities of chemosymbiotic microbial communities (Roberts and Feng, 2013). These processes are tightly linked to biogeochemical turnover and the combination of downward-diffusing seawater and upward advection of hydrocarbon-rich pore fluids (Roberts and Aharon, 1994; Sassen et al., 2004; Roberts and Feng, 2013; Suess, 2018). Furthermore, chemosymbiotic benthic biota are supported by microbially-driven anaerobic oxidation of methane (AOM), which involves a microbial consortium of anaerobic methanotrophic archaea (ANME) and sulfate-reducing bacteria (SRB). AOM anaerobically oxidizes methane while reducing sulfate to sulfide

at the sulfate-methane transition zone (SMTZ), with the following net reaction (Boetius et al., 2000):

$$CH_4 + SO_4^{2-} \rightarrow HCO_3^- + HS^- + H_2O. \qquad (1)$$

Bicarbonate (HCO_3^-) from the process enters the dissolved inorganic carbon (DIC) pool in shallow sediments. Authigenic carbonates are common early diagenetic precipitates formed at methane and other hydrocarbon seep sites (Aloisi et al., 2002; Naehr et al., 2007). They are formed primarily through bicarbonate production via AOM, which results in supersaturation of carbonate ions with respect to carbonate minerals in porewater at the SMTZ and induces carbonate precipitation (Baker and Burns, 1985; Ritger et al., 1987, Eq. 2):

$$2HCO_3^- + Ca^{2+} \rightarrow CaCO_3 + CO_2 + H_2O. \qquad (2)$$

Carbonate authigenesis at seep sites is a substantial carbon sequestration process and provides an excellent geologic archive of diagenetic geochemical reactions involving both carbon and sulfur at seeps. At present-day settings, for example, authigenic carbonate precipitation is considered to be a significant component of the marine carbon sink (Wallmann et al., 2008; Torres et al., 2020), accounting for 10-15% carbonate accumulation in pelagic and neritic sediments (Sun and Turchyn, 2014; Akam et al., 2020). Further, carbon sequestration due to authigenic carbonate formation may have played an even larger role in geological past, especially during periods of widespread oceanic anoxia (Schrag et al., 2013). The first-order pathways and processes in the cycles of C, S, and other elements are relatively well constrained for modern seep sites. However, much of the detail, magnitude, and variability of these biogeochemical processes as well as their impacts on geological carbon budgets are still unclear. A better understanding of seep-associated C-S coupling is of great importance in recognizing the role of these processes on the ancient Earth, including relationships to Oceanic Anoxic Events and early evolution of oxygen in Earth's atmosphere (Higgins et al., 2009; Bristow and Grotzinger, 2013; Canfield and Kump, 2013; Havig et al., 2017).

Studies of organic biomarkers in sediments from the GoM (Pancost et al., 2005) revealed disparities between measured rates of sulfate reduction versus methane oxidation that suggest other carbon sources in addition to methane (Joye et al., 2004; Bowles et al., 2011). Further, carbon isotope data from authigenic carbonates (Formolo et al., 2004) also suggest that AOM

may not be the only process responsible for an increase in carbonate alkalinity at many seep sites. Rather, it seems likely that the anaerobic oxidation of non-methane hydrocarbons (AONM) coupled with sulfate reduction (Widdel and Rabus, 2001; Kniemeyer et al., 2007; e.g., hexadecane, Eq. 3, propane, Eq. 4) provides a significant source of metabolic energy and bicarbonate at these locations (Formolo et al., 2004; Joye et al., 2004; Naehr et al., 2009; Mansour and Sassen, 2011; Smrzka et al., 2019; Sun et al., 2020).

$$C_{16}H_{34} + 12.25\ SO_4^{2-} \rightarrow 16\ HCO_3^- + 12.25\ HS^- + 3.75\ H^+ + H_2O \quad (3)$$

$$4\ C_3H_8 + 5\ SO_4^{2-} \rightarrow 6\ HCO_3^- + 5\ HS^- + 4\ H_2O + H^+ \quad (4)$$

Even though seeps dominated by heavy hydrocarbons (like crude oil) are less common than seeps dominated by light hydrocarbons (like methane), their occurrences are well documented globally (e.g., Hornafius et al., 1999; Noble et al., 2009; Valentine et al., 2010; Jones et al., 2014; Körber et al., 2014; Jiang et al., 2018) and suggest an important effect on microbial diversity and associated biogeochemical cycling (Joye et al., 2004; Orcutt et al., 2010; Sahling et al., 2016). For example, GoM hydrocarbon seeps have been shown to supply subsurface-derived microbial populations, biomass, and metabolic potential along with the geofluids to deep ocean (Chakraborty et al., 2020), significantly impacting the biogeochemistry of shallow sediments (Hovland et al., 2012; Coffin et al., 2013; Rowe, 2017) as well as the overlying water column (D'souza et al., 2016). Oil seeps almost certainly have persisted over geologic time (Wilson et al., 1974) and are relevant to ocean chemistry over the same time scales. Characterizing and comparing the impacts of crude oil and methane seeps in present-day settings will enable better identification of these processes in the sediment record and their biogeochemical implications over geologic time (Peckmann and Thiel, 2004; Campbell, 2006; Bristow and Grotzinger, 2013). Furthermore, hydrocarbon seeps are highly sensitive in response to changes in oceanographic and tectonic conditions (e.g., Aharon et al., 1997; Berndt et al., 2014; Oppo et al., 2020), and our current understanding of their temporal variation is weak. Such uncertainty also leaves a critical gap in our ability to assess the potential response of these seep systems during future climate change.

In this study, we examined authigenic carbonates using carbon ($\delta^{13}C_{CaCO3}$), oxygen ($\delta^{18}O_{CaCO3}$), and sulfur isotopes ($\delta^{34}S$ of chromium reducible sulfur – CRS) along with the carbonate-

associated sulfate (CAS) to examine the geological signatures of methane and crude oil oxidation (e.g., Eq. 3). CRS represents total reduced inorganic sulfur (pyrite S + acid-volatile sulfide S + elemental S), with the exclusion of organic S and sulfate phases (Canfield et al., 1986). This fraction is typically but not always dominated by pyrite in most sediments (Lyons, 1997; Rickard et al., 2017). We focused our attention on the authigenic carbonates recovered from asphalt seep sites in Chapopote Knoll of Campeche Bay, which were suggested to be dominantly derived from crude oil oxidation. The study site is characterized by extensive and serial asphalt flows, oil and gas seeps, and seafloor gas hydrate deposits, along with seep-associated chemosynthetic communities and authigenic carbonate deposits (MacDonald et al., 2004; Brüning et al., 2010; Sahling et al., 2016). These discoveries added a new dimension to the inventory of seafloor hydrocarbon seep processes (Bohrmann, 2014; Marcon et al., 2018). Given this importance, we compared the results from Chapopote seep carbonates with multiple seep sites from the northern Gulf of Mexico, many of which are methane-dominated seeps devoid of oil. As part of this study, we determined U-Th dates for the Chapopote seep carbonate to identify the timing and mechanisms of formation.

2. Study Area

The GoM basin is characterized by multiple, and often large hydrocarbon reservoirs commonly overlying salt deposits, which are sealed by overlying continental margin sediments. Differential sedimentary loading and density contrast with the overburden induce salt diapirism and consequent fault generation, paving the way for hydrocarbon leakages toward seafloor (Brooks et al., 1990; Sassen et al., 1993; Roberts, 2001; Fisher et al., 2007; Kennicutt, 2017). The southern GoM is a relatively unexplored area with numerous hydrocarbon seeps and is characterized by two distinct active salt provinces: the Campeche and Sigbee Knolls, separated from the Mississippi-Texas-Louisiana salt province in the northern GoM by the Sigsbee Abyssal Plain (Bryant et al., 1991; Fig. 1). These knolls consist of a series of domes and ridges formed by movement of the Jurassic salt deposits underlying the ~5 to 7 km thick continental margin sediments (Salvador, 1991; Ding et al., 2008). Extensive hydrocarbon transport from sediments to the sea-surface in the region is observable via satellite images as sea-surface oil slicks (MacDonald et al., 2004; MacDonald et al., 2015; Suresh, 2015; Römer et al., 2019).

This study employs carbonate samples collected at a water depth of 2902 m from Chapopote Knoll (21°54′N/93°26′W) located on the northern slope of the Campeche Knolls province during the *R/V Sonne* cruise SO174/2 in 2003 (Bohrmann and Schenck, 2004) and *R/V Meteor* cruise M67/2 in 2006 (Bohrmann et al., 2008). The Campeche Knolls province consists of a cluster of elongated knolls and ridges formed via salt tectonics (Garrison and Martin, 1973). The knolls have relief ranging from 450 to 800 m above the seafloor in water depths of 3000 to 3500 m (Ding et al., 2008). A gravity core GeoB 10602 collected about 50 m away from the asphalt flow, which did not contain any oil, asphalt, or $CaCO_3$ crusts serves as non-seep background sample for Chapopote seep site (Fig. 1C).

Extensive and overlapping lava-like asphalt flows at Chapopote emanate from a central crater-like depression, generating extensive surface deposits of solidified asphalt with distinct surface textures—leading to the term 'asphalt volcano' (MacDonald et al., 2004). Seismic studies revealed that asphalt seeps derive from a large reservoir buried at shallow depths linked to a deep, heavy petroleum source (Ding et al., 2008; Ding et al., 2010). Asphalt flow is accompanied by oil and gas seeps (Bohrmann, 2008) and seafloor gas hydrate deposits (Klapp et al., 2010), along with seep-associated chemosymbiotic communities and authigenic carbonate deposits (Bohrmann and Schenck, 2004; MacDonald et al., 2004; Naehr et al., 2009; Brüning et al., 2010; Sahling et al., 2016). Seepage systems support prolific microbial activity involving crude oil degradation and sulfate reduction (Schubotz et al., 2011a; Schubotz et al., 2011b) in otherwise deep sea pelagic sediments with low organic carbon input from surface waters. Surface sediments from Chapopote are characterized by locally higher total organic carbon contents (0.9%) and very high carbon-nitrogen atomic ratios (C/N_a) compared to the surrounding abyssal sediments (ratios of 50 vs. 7), suggestive of organic carbon sourced from hydrocarbon seepage rather than deposition (Escobar-Briones and García-Villalobos, 2009). Authigenic carbonates collected from Campeche seeps allow us to investigate the role of crude oil oxidation during carbonate authigenesis (Naehr et al., 2009; Smrzka et al., 2016).

For comparison, we also analyzed samples from relatively well-studied sites of northern continental slope of GoM Green Canyon Block 415 (GC 415, 27°33.48N/90°58.86W, water depths 950m; 27°32.61N/90°59.54W, water depth 1045m) and Bush Hill (GC 185, 27°46.97N/91°30.47W, water depths 547m). These sites were also among the expedition targets

of *R/V Sonne* cruise 174 (Bohrmann and Schenck, 2004; Fig. 1). Similar to Campeche Knolls, these sites host widespread hydrocarbon seeps due to fractures in sedimentary strata induced by salt tectonics (Roberts and Aharon, 1994; Sassen et al., 2004; Feng et al., 2009). Our preliminary analysis along with previous reports revealed a noticeable contribution of crude oil oxidation to the DIC pool at GC 185 and methane oxidation to DIC pool at GC 415 (Sassen et al., 1994; Akam et al., 2019). Further, we used published literature reports of C-S isotope values for seep carbonates collected from multiple sites in the northern GoM (Atwater Valley - AT340, Green Canyon – GC 180, GC 232, GC 234, GC 852 Garden Banks – GB 260, GB 382, GB 427, GB 647, and Mississippi Canyon MC 118, Fig. 1) (Formolo and Lyons, 2013; Feng et al., 2016; Sun et al., 2020). Among these sites, GC 232 serves as a representation of a crude oil-dominant site (Sun et al., 2020), and other sites represent either methane-dominant settings or a mix of methane and crude oil seepage. Near-surface sediments (0-10 cm below seafloor) collected from approximately 2.6 km north of a brine pool at GC233 and away from any visible hydrocarbon seeps serve as a background site for the northern GoM (Formolo and Lyons, 2013). Table 1 summarizes the data sources for this study. We also emphasize that all the samples analyzed in this study and retrieved from literature for comparison are from surface/near-surface sediments of the seafloor, thus placing our emphasis on the earliest diagenetic processes.

Table 1: Location, water depth, and seep type of the samples studied.

Data Source	Site	Approximate Location	Water depth (m)	Seep type
This study	Chapopote Knoll	21°54.0N, 93°26.40W	2902	Crude oil dominant
	Bush Hill GC 185	27°46.97N, 91°30.47W	547	Crude oil dominant
	GC 415	27°32.61N, 90°59.54 W	1045	Methane and crude oil
	GC 415	27°33.48N, 90°58.86W	950	Methane and crude oil
	Chapopote Background	21°54.01N, 93°26.24W	2884	No seep
Feng et al. (2016) and Sun	AT340	27°38.8N, 88°21.9W	2216	Methane dominant

et al. (2020)	GB260	27°42.5N, 91°58.5W	503	Methane dominant
	GB427	27°35.50N, 92°25.94W	853	Methane and crude oil
	GB647	27°20.50N, 92°24.18W	950	Methane and crude oil
	GC140/184	27°49.16N, 91°31.95W	287	Methane and crude oil
	GC180	27°28.2N, 91°18.0W	253	Methane and crude oil
	GC232	27°44.50N, 91°19.28W	537	Crude oil dominant
	GC238	27°44.45N, 91°03.05W	728	Methane dominant
	GC852	27°6.36N, 91°9.97W	1633	Methane dominant
	MC118	27°06.3N, 91°09.8W	885	Methane and crude oil
Formolo and Lyons (2013)	GC 234	27°44.79N, 91°13.33W	550	Methane and crude oil
	Northern GoM Background	27°43.42N, 91°19.09W	716	No seep

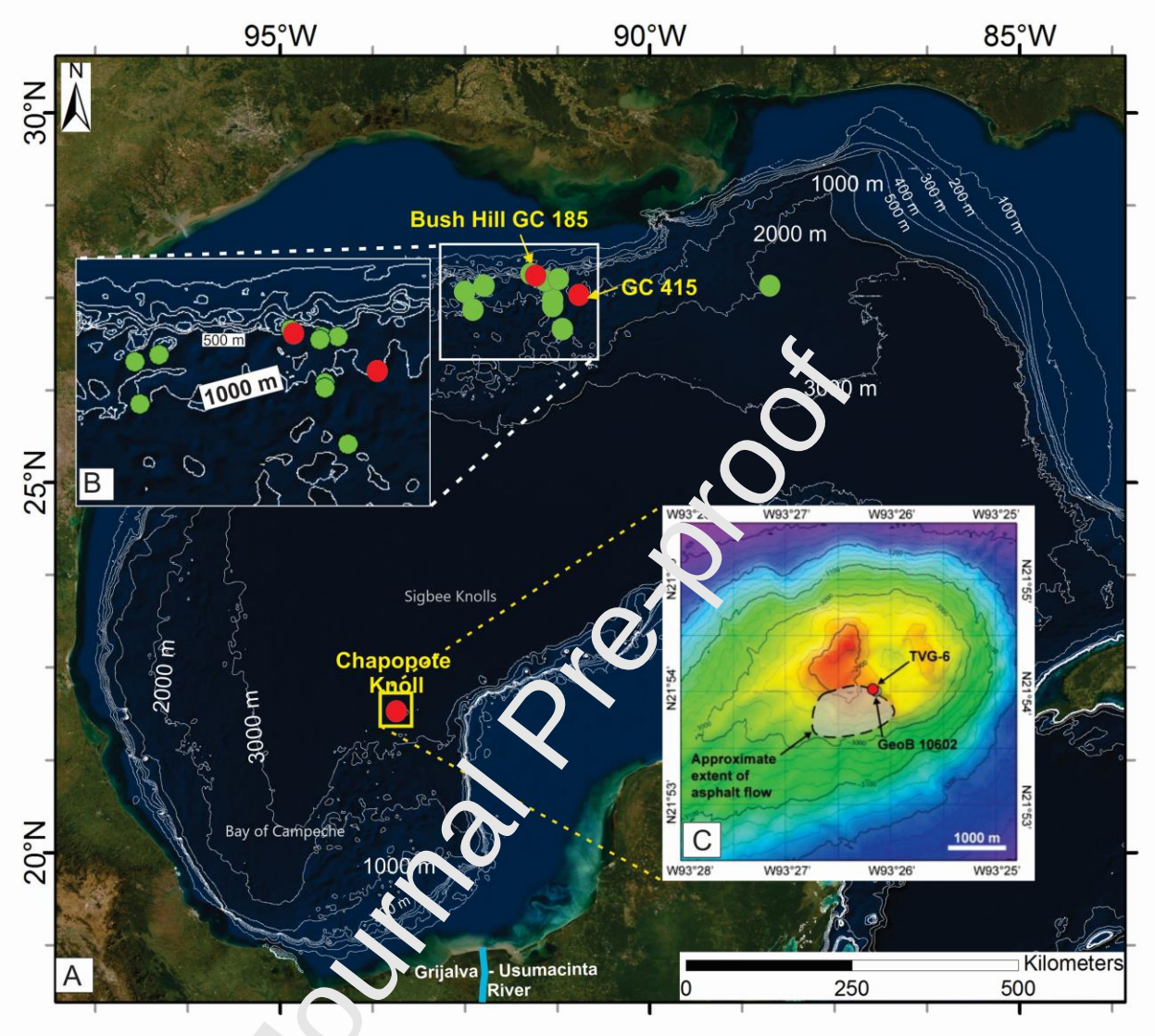

Figure 1: A) Map of the Gulf of Mexico (GoM) showing locations of the study site at Chapopote Knoll and other sites considered within this study within the northern GoM (GC 415 and GC 185). Significant asphalt seepage occurs at Chapopote Knoll whereas the northern GoM sites show a mixture of methane and oil seepage. The green dots indicate locations from published literature where we used those C-S isotopic data for comparison with that from Chapopote Knoll. B) A magnified view of northern GoM sites for an overview of bathymetry. C) A magnified view of Chapopote knoll with 25 m bathymetric contours modified from Naehr et al. (2009). This study uses seep carbonates collected from TVG-6 site (red dot) and background sediment

samples collected from GeoB 10602 (dark gray dot). Light gray shading represents an approximate extent of asphalt flow.

3. Methods

Carbonate samples were collected from surface sediments via video-guided grab sampling. Authigenic carbonate crusts and shell material from chemosynthetic clams were separated from grab samples. Specific samples were defined based on the dive number and location. Fifteen carbonate crusts were analyzed, which included ten crusts from Chapopote (different pieces from three large grab samples, sample ID TVG6 22 -30), four irregular tabular crusts from GC 185 (sample ID GC 185N1-3, N10), and a tabular concretion from GC 415 (sample ID GC 415T). These materials were split into multiple subsamples based on observations from hand specimens. Carbonate content of the samples were determined by acid-leaching/weight-loss procedure and are reported as weight percent $CaCO_3$. Bulk mineralogy was determined by X-ray diffraction (XRD) according to Naehr et al. (2000) at TAMUCC. One gram of crushed sample was mixed with 0.25 gm internal corundum standard (α-Al_2O_3) to prepare randomly-oriented powdered slides. Scans were run from 20°- 60° using a Rigaku Ultima III X-ray diffractometer at TAMUCC at a scan speed of 0.01° 2θ/s. Relative proportion of magnesium content in carbonate was determined using the shift d spacing of the reflection (104) (Greinert et al., 2001). Calcite with $MgCO_3$ <4% is referred to as low-Mg calcite, and 4-30% were considered high-Mg calcite (Flügel, 2004). Polished thin sections 50 x 75 mm in size, partially stained with alizarin red and potassium ferrocyanide, were used for textural and compositional analysis via standard optical microscopy. Stable isotopes of carbon and oxygen from authigenic carbonates were determined using a ThermoScientific Gasbench Device coupled to a Delta V Advantage Isotope Ratio Mass Spectrometer (IRMS) via a ConFlo IV inlet at the University of California, Riverside. Sample powders were microdrilled from polished slab surfaces for bulk micritic carbonate subsamples (microdrilled samples for each crust were named as A-D in Table 2). Carbon dioxide for $\delta^{13}C_{CaCO3}$ and $\delta^{18}O_{CaCO3}$ analyses was produced by reaction of samples with 103% orthophosphoric acid. Precision of $\delta^{13}C_{CaCO3}$ and $\delta^{18}O_{CaCO3}$ measurements is 0.2‰. The $\delta^{13}C_{CaCO3}$ and $\delta^{18}O_{CaCO3}$ are reported with reference to Vienna Pee Dee Belemnite (VPDB) standard.

U/Th analyses were performed on samples micro-drilled from polished samples targeted for early diagenetic, particularly micritic, cements. Thirty samples were initially screened for $^{238}U/^{232}Th$ ratios to determine whether they could be dated by U/Th methods. One milligram of sample was dissolved in 1.5 mL 0.5 M nitric acid, and U, Th, and Ca were measured by quadrupole ICP-MS at the MIT Center for Environmental Health Sciences to determine U concentrations and U/Th ratios. A gravimetric U/Th/Ca solution with similar abundances to the samples was used to calibrate the instrument, and a standard was run after every 15-20 samples to monitor instrument drift. Samples with $^{238}U/^{232}Th$ mass ratios greater than two were selected for U/Th dating analysis. Radioactive U/Th isotope dating of the carbonate crusts was performed Nu Plasma II-ES MC-ICP-MS at the Department of Earth, Atmospheric and Planetary Sciences, Massachusetts Institute of Technology (MIT). Micro-drilled carbonate powder samples ranging in weight from 10 to 70 mg were used. Samples were dissolved in 8 N HNO_3 and spiked with a $^{229}Th/^{233}U/^{236}U$ tracer. Uranium and Th were separated following procedures described by Edwards et al (1987) and Bayon et al., (2009). Raw data were corrected with an initial $^{230}Th/^{232}Th$ atomic ratio of $4.4 \pm 2.2 \times 10^{-6}$, assuming a typical upper continental crust value for $^{238}U/^{232}Th$, and the errors were arbitrarily assumed to be 50%. This initial $^{230}Th/^{232}Th$ ratio is consistent with values used in some prior studies of seep carbonates from the GoM and other areas (Feng et al., 2010; Chen et al., 2019), but we note that Aharon et al. (1997) used initial $^{230}Th/^{232}Th$ ratios ranging from 8.2×10^{-6}. Use of a higher initial $^{230}Th/^{232}Th$ ratio would result in younger corrected ages; we note the need for future work to better constrain this ratio at our site. $\delta^{234}U_{initial}$ was calculated based on ^{230}Th age (T), that is, $\delta^{234}U_{initial} = \delta^{234}U_{measured} \times e^{\lambda 234 * T}$, and T is the corrected age. Decay constants for ^{230}Th and ^{234}U are from Cheng et al. (2013); the decay constant for ^{238}U is 1.55125×10^{-10} yr^{-1} (Jaffey et al., 1971).

Carbonate associated sulfate (CAS) was extracted on micro-drilled samples targeted for micritic and early diagenetic cements using a technique modified from Lyons et al (2004). This method includes removal of initial sulfate salts (before acid addition) with a NaCl solution and treatment for sulfides and organically bound sulfur (e.g., ester bound sulfates) using a 5% sodium hypochlorite rinse. Furthermore, 5% (by weight) $SnCl_2$ was used to inhibit pyrite oxidation during the 4N HCl treatment. Despite these precautions, our attempt to measure CAS in Chapopote samples failed, yielding many highly negative $\delta^{34}S_{CAS}$ values rather than the positive values from seawater and as modified via microbial sulfate reduction. We attribute these

problems to extremely low CAS concentrations (as low as 31 ppm) and concomitant vulnerability to any sulfide oxidation during extraction, as well as residual sulfate derived from sulfide during sample collection, storage, or naturally prior to collection. Thus, our CAS data are not valid because of extremely low concentrations and are not reported.

Chromium reducible sulfur (CRS) from bulk micritic carbonate samples was extracted using a modified method of Canfield et al (1986) . Homogenized 5 g samples were reacted with 10 ml ethanol, 25 ml of 6M HCl, and 25 ml of a chromium chloride (1 M $CrCl_3.6H_20$ in 0.5 M HCl) solution. CRS was converted to H_2S gas and carried via a N_2 carrier gas to an $AgNO_3$-NH_4OH trap where it was quantitatively converted to silver sulfide (Ag_2S). Ag_2S precipitates were recovered on polycarbonate membrane filters using vacuum filtration before being dried and weighed to determine the CRS weight percent. $\delta^{34}S_{CRS}$ values were measured using a Thermo Scientific Delta V Plus IRMS connected to a Costech 4010 ECS via a ConFlo III interface at the University of California, Riverside. Standard deviation for $\delta^{34}S$ analysis was ± 0.23‰ (VCDT).

A cluster analysis of the $\delta^{13}C_{CaCO3}$ and $\delta^{34}S_{CRS}$ data pairs was performed on data obtained from this study along with the data collected from published literature from additional sites mentioned in Table 1 (Supp. Table 1) via *k*-means unsupervised learning algorithm using Python. This approach allowed an additional tool to classify the $\delta^{13}C_{CaCO3}$ and $\delta^{34}S_{CRS}$ data pairs, along with classification using seep types mentioned in Table 1. K-means divides objects into clusters that show similar characteristics and are dissimilar to the objects belonging to another cluster. The elbow method, which fits the models with a range of values of k (number of clusters), was used to determine the optimum value of k. Visual inspection of spread of the data and the site characteristics were also considered here to choose the optimal k value. Once k is determined, each data point is assigned to a cluster based on minimizing the distance between the points within a cluster. The final field boundaries to classify the $\delta^{13}C_{CaCO3}$ and $\delta^{34}S_{CRS}$ data pairs were delineated by combining cluster density and site characteristics (seep type, Table 1).

4. Results

4.1 Petrography

Petrographic observations of carbonate macro- and microfacies from Chapopote seep carbonates were previously reported by Canet et al., (2006) and Naehr et al (2009). Aragonite was the primary phase for Chapopote seep carbonates. The siliciclastic components consisted of detrital quartz, feldspar, and clay minerals. Petrographic observations of the samples showed wide-ranging textural variations (Figure 2). Aragonite cement types included acicular, botryoidal, peloidal, micritic, and sparitic cement. Microsparitic aragonite was the volumetrically dominant phase, commonly occurring as peloidal and clotted textures. Aragonite crystals were often coated with crude oil residues. Macroscopically, the samples consisted of irregularly-shaped large clasts that were held together by a microsparitic to sparitic aragonite cement. The clasts were composed of lithic (primarily mud- and siltstones) and biogenic components (primarily bivalve and foraminifera shells). Primary pore space was widespread resulting from incomplete filling of voids between clasts and microsparitic or fibrous cements (Fig. 2B). Secondary pores, potentially caused by carbonate dissolution and *in situ* brecciation, were also observed (Fig. 2A). Framboidal pyrite was pervasive (Fig. 2F).

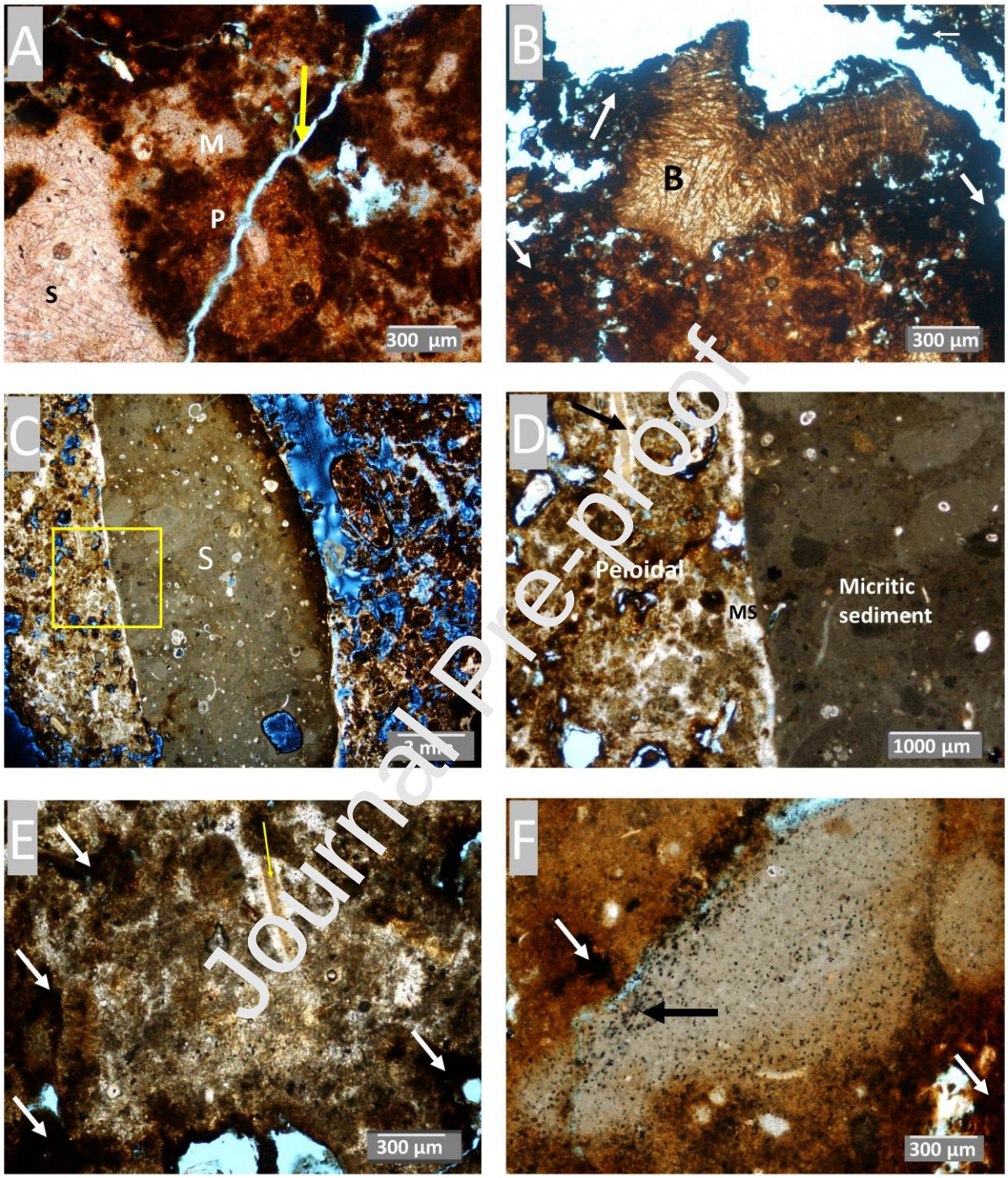

Figure 2: Petrographic observations on Chapopote seep carbonates. All images are in plane-polarized light, and blue color indicates pore spaces. A) Multiple cement types including peloidal (P), Sparitic (S), and micritic (M) cement. Note fracture (arrow) post-dating cement formation. B) Banded and botryoidal aragonite (B) that also exhibits fibrous and needle-like

crystals. C) Sediment (S) cemented by microcrystalline and peloidal aragonite. Yellow box is enlarged in D. D) Zoomed view of yellow box of C. Microsparite (MS) filling of spaces between sediments and cement surrounding the clasts is incomplete, leaving significant pore space . Aragonite cement fills pore spaces, creating a peloidal texture in the left half of the picture. A bivalve shell fragment (black arrow) is visible. E) Peloidal texture suggestive of microbial activity and early diagenetic cementation. A shell fragment (yellow arrow) and oil coatings (white arrows) are visible. Oil coating (white arrows) surrounding the aragonite cement can be seen. F) Pyrite clumps (black arrow) composed of pyrite framboids approximately 15 to 20 μm in size is suggestive of sulfate reduction. Clots of residual hydrocarbons (white arrow) can be seen around the pore spaces adjacent to cemented structures as well as coating on the aragonite cements.

4.2 U-Th dates

Of the 30 samples screened for U-Th dating, nine Chapopote samples had $^{238}U/^{232}Th$ greater than 2, and are thus suitable for age-dating. These samples were analyzed for U/Th isotopic composition and age dated (Table 2). The ^{238}U concentrations for these selected samples ranged from 5230 to 13200 ppb, and ^{232}Th concentrations ranged from 482 to 1220 ppb. $\delta^{234}U$ initial values averaged 143‰ when corrected for detrital U (based on an initial $^{230}Th/^{232}Th$ atomic ratio of $4.4 \pm 2.2 \times 10^{-6}$ and assuming that $^{230}Th/^{238}U$ and $^{234}U/^{238}U$ activity ratios in detrital matter are 1 ± 0.1). The initial $\delta^{234}U$ values of the carbonate fraction of the Chapopote samples is 147 ± 1‰, consistent with the average seawater composition of 146.8 ± 0.1‰ (Andersen et al., 2010). U-Th dates ranged from 4.6 ± 1.0 ka to 13.5 ± 2.1 ka (BP). $^{230}Th/^{232}Th$ atomic ratios were between 11.4×10^{-6} and 19.0×10^{-6}, making corrections for initial ^{230}Th large. As a result, uncertainties in the corrected ages are dominated by the uncertainty in the initial ^{230}Th correction.

Table 2: U-Th data from Chapopote samples

Sample ID	^{238}U ±	^{232}Th ±	$^{230}Th/^{232}Th$	$\delta^{234}U$ (‰)	$^{230}Th/^{238}U$	^{230}Th Age (ka BP)	^{230}Th Age (ka	$\delta^{234}U$ initial

	(2σ)[a] (ppb)	(2σ)[a] (ppb)	± (2σ) (atomic ×10^{-6})	± (2σ)[b] (measured)	± (2σ) (activity)	± (2σ)[c] (uncorrected)	BP) ± (2σ)[d,e] (corrected)	(‰) ± (2σ)[f] (corrected)
TVG_6-21a	13150 ± 260	1183 ± 24	19.0 ± 0.3	143 ± 2	0.1074 ± 0.0017	10.788 ± 0.19	8.32 ± 1.2	146 ± 2
TVG_6-23a	6673 ± 133	1060 ± 21	13.4 ± 0.3	138 ± 0.3	0.1340 ± 0.0029	13.750 ± 0.32	9.40 ± 2.2	141 ± 3
TVG_6-25a	7253 ± 145	1104 ± 22	11.6 ± 0.3	138 ± 0.3	0.1109 ± 0.0028	11.260 ± 0.31	7.10 ± 2.1	140 ± 2
TVG_6-26a	7799 ± 156	1163 ± 23	18.0 ± 0.3	139 ± 0.3	0.1691 ± 0.0028	17.670 ± 0.33	13.50 ± 2.1	143 ± 2
TVG_6-26c	5231 ± 105	1018 ± 20	13.7 ± 0.3	137 ± 0.3	0.1673 ± 0.0036	17.460 ± 0.41	12.10 ± 2.8	141 ± 3
TVG_6-27a	7736 ± 155	1074 ± 22	14.1 ± 0.3	142 ± 0.3	0.1235 ± 0.0026	12.630 ± 0.29	8.79 ± 1.9	144 ± 2
TVG_6-27c	6824 ± 482	482 ± 10	14.8 ± 0.3	143 ± 0.3	0.0659 ± 0.0014	6.507 ± 0.15	4.55 ± 0.96	144 ± 2
TVG_6-28a	5990 ± 120	993 ± 20	15.4 ± 0.3	140 ± 0.3	0.1612 ± 0.0031	16.700 ± 0.35	12.10 ± 2.3	144 ± 2
TVG_6-29d	10160 ± 200	1221 ± 24	11.4 ± 0.3	142 ± 0.3	0.0864 ± 0.0022	8.630 ± 0.23	5.32 ± 1.67	144 ± 2

Notes:

Decay constants for ^{230}Th and ^{234}U are from Cheng et al. (2013); decay constant for ^{238}U is 1.55125 x 10^{-10} yr^{-1} (Jaffey et al., 1971).

[a]Reported errors for ^{238}U and ^{232}Th concentrations are estimated to be ±1% due to uncertainties in spike concentration; analytical uncertainties are smaller.

[b] $\delta^{234}U = ([^{234}U/^{238}U]_{activity} - 1) \times 1000$.
[c]$[^{230}Th/^{238}U]_{activity} = 1 - e^{-\lambda 230 T} + (\delta^{234}U_{measured}/1000)[\lambda_{230}/(\lambda_{230} - \lambda_{234})](1 - e^{-(\lambda 230 - \lambda 234) T})$, where *T* is the age. "Uncorrected" indicates that no correction has been made for initial ^{230}Th.

[d]Ages are corrected for detrital ^{230}Th assuming an initial $^{230}Th/^{232}Th$ of (4.4 ± 2.2) x 10^{-6}.

[e]B.P. stands for "Before Present" where the "Present" is defined as January 1, 1950 C.E.
[f] $\delta^{234}U_{initial}$ corrected was calculated based on ^{230}Th age (T), i.e., $\delta^{234}U_{initial} = \delta^{234}U_{measured} \times e^{\lambda 234 * T}$, and T is corrected age.

4.3 C-O and S isotopes

Our measured values of $\delta^{13}C_{CaCO3}$, $\delta^{18}O_{CaCO3}$, and $\delta^{34}S_{CRS}$ are shown in Table 2. $\delta^{13}C_{CaCO3}$ and $\delta^{18}O_{CaCO3}$ values from Chapopote samples averaged -25‰ and +4.5‰, respectively. Samples from the northern GoM, GC 185 and GC 415, yielded average $\delta^{13}C_{CaCO3}$ values of -19.8‰ and 4.4‰ and $\delta^{18}O_{CaCO3}$ values of -34.6‰ and +4.8‰, respectively (Fig. 3A; Table 2). $\delta^{34}S_{CRS}$ values from Chapopote carbonates were noticeably low, ranging from -14‰ to -38.7‰, with an average value -27.4‰. Samples from GC 415 and GC 185 averaged -4.8‰ and +18.9‰, respectively. Data for additional sites compiled from literature is summarized in supplementary Table 1. Overall, the $\delta^{13}C_{CaCO3}$, $\delta^{18}O_{CaCO3}$, and $\delta^{34}S_{CRS}$ data showed noticeable spread within and between the sites (Fig. 3B-D).

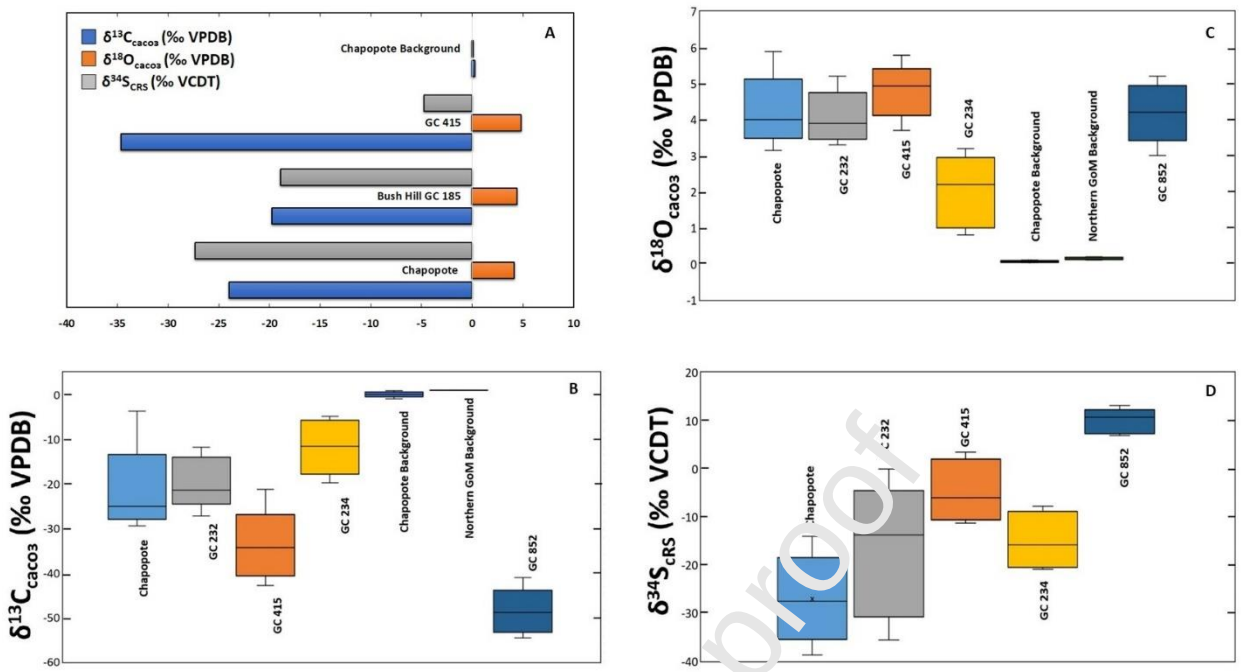

Figure 3: A) Average values of $\delta^{13}C_{CaCO3,}$ $\delta^{18}O_{CaCO3,}$ and $\delta^{34}S_{CRS}$ obtained from samples in this study. B-D: Box and whisker plot for $\delta^{13}C_{CaCO3}$ (Fig. 3B), $\delta^{18}O_{CaCO3}$ (Fig. 3C), and $\delta^{34}S_{CRS}$ (Fig. 3D) from seven sites (Chapopote, GC 232, GC 415, GC 234, GC 852, Chapopote Background and northern GoM background) that shared 83% of the total data in this study which includes new data and that compiled from literature. Refer to Table 1 for site descriptions. Note that the near-surface (<10 cmbsf) background samples from Chapopote and northern GoM did not yield measurable CRS content.

Table 2: $\delta^{13}C_{CaCO3,}$ $\delta^{18}C_{CaCO3}$, and $\delta^{34}S_{CRS}$ values, with chromium reducible sulfur (CRS) and calcium carbonate ($CaCO_3$) content from studied samples. Sample materials involve authigenic carbonate crusts, shell material at seep sites and surface sediments of background sites. An extended database, which includes a compilation of published literature data from multiple seep sites in GoM, is provided in Supplementary Table 1.

Location	Water depth (m)	Sample ID	$CaCO_3$ (wt %)	CRS (wt %)	$\delta^{13}C_{CaCO3}$ (‰ VPDB)	$\delta^{18}O_{CaCO3}$ (‰ VPDB)	$\delta^{34}S_{CRS}$ (‰ VCDT)	Mineralogy

Chapopote Knoll 21°54.0N, 93°26.40W	2902	TVG-6 22A	96%	0.01 %	-25.0	4.2	-20.1	Aragonite
		TVG-6 22B	90%	0.05 %	-24.8	3.8	-26.2	Aragonite
		TVG-6 22C	97%	0.06 %	-24.5	4.6	-19	Aragonite
		TVG-6 22D	91%	0.00 %	-24.1	4.4	-18.8	Aragonite
		TVG-6 23A	84%	0.12 %	-27.6	5.7	-28	Aragonite
		TVG-6 23B	88%	0.17 %	-26.2	3.8	-23.7	Aragonite
		TVG-6 23C	70%	trace	-26.9	3.7	-22.0	Aragonite
		TVG-6 24B	87%	0.36 %	-25.0	5.9	-27.3	Aragonite
		TVG-6 24C	85%	0.17 %	-26.3	4.4	-28.5	Aragonite
		TVG-6 24D-SHELL	70%	0.00 3%	-4.1	3.3	-27.5	Aragonite
		TVG-6 25A	87%	0.21 %	-24.2	4.1	-27.6	Aragonite
		TVG-6 25B	70%	0.53 %	-25.7	5.1	-24.4	Aragonite
		TVG-6 26A	99%	0.08 %	-26.5	4.3	-21.7	Aragonite
		TVG-6 26B	81%	0.26 %	-25.0	5.3	-21.6	Aragonite
		TVG-6 26C	83%	0.16 %	-25.6	4.3	-28.5	Aragonite
		TVG-6 27A	87%	0.08 %	-26.0	4.0	-34.8	Aragonite
		TVG-6 27B	75%	0.38 %	-28.5	4.5	-33.4	Aragonite
		TVG-6 27C	87%	0.14 %	-23.3	4.3	-33.4	Aragonite
		TVG-6 28A	64%	0.06 %	-26.3	4.0	-31.3	Aragonite
		TVG-6 28B	89%	0.02 %	-25.8	4.7	-38.4	Aragonite
		TVG-6 28C	71%	0.02 %	-25.2	4.4	-26.5	Aragonite
		TVG-6 28D-SHELL	96%	0.07 %	-23.0	4.3	-33.1	Aragonite
		TVG-6 29B	96%	0.21	-25	4.6	-27.4	Aragonit

				%				e
		TVG-6 29C	99%	0.48 %	-27.4	4.9	-38.7	Aragonite
		TVG-6 29F	91%	0.01 %	-26.9	3.9	-34.9	Aragonite
		TVG-6 30A	88%	0.47 %	-26.8	5.6	-27.6	Aragonite
		TVG-6 30B	85%	1.04 %	-29.4	5.1	-14.1	Aragonite
Chapopote Background 21°54.01N, 93°26.24W	2884	GeoB BGA	33%	trace	0	0.09	-	NA
		GeoB BGB		trace	1	0.07	-	NA
		GeoB BGC		trace	-1	0.05	-	NA
		GeoB BGD		trace	0.9	0.04	-	NA
		GeoB BGE		trace	0.3	0.10	-	NA
GC 185 27°46.97N, 91°30.47W	547	GC 185 N10A1	80%	0.23 %	20.9	5.2	-18.5	HMC
		GC 185 N10A2	84%	0.63 %	-21.4	4.6	-18.5	HMC
		GC 185 N10B1	71%	0.10 %	-16.3	4.2	-24.2	HMC
		GC 185 N10B2	54 %	0.44 %	-20.5	3.8	-14.5	HMC
GC 415 27°32.61N, 90°59.54 W	1045	GC 415 N1-A	69%	0.17 %	-32.0	5.8	-7.4	HMC
		GC 415 N1-B	83%	0.44 %	-27.4	5.0	-4.7	HMC
		GC 415 N2-A	74%	0.48 %	-31.3	5.6	-11.3	HMC
		GC 415 N2-B	74%	0.74 %	-39.3	4.9	-10.9	HMC
		GC 415 N3-A	68%	0.07 %	-24.3	4.7	2.3	HMC
		GC 415 N3-B	62%	0.10 %	-21.3	5.0	3.4	HMC
GC 415 27°33.48N, 90°58.86W	951	GC 415 T-1	90%	N/A	-35.14	5.09	N/A	HMC
		GC 415 T-2	85%	N/A	-34.30	5.05	N/A	HMC
		GC 415 T-3	91%	N/A	-37.78	5.40	N/A	HMC
		GC 415 T-4	89%	N/A	-36.73	3.70	N/A	HMC
		GC 415 T-5	92%	N/A	-32.97	4.38	N/A	HMC
		GC 415 T-6	96%	N/A	-34.12	4.28	N/A	HMC
		GC 415 T-7	91%	N/A	-34.29	3.90	N/A	HMC
		GC 415 T-8	88%	N/A	-37.60	3.94	N/A	HMC
		GC 415 T-9	91%	N/A	-42.3	4.9	N/A	HMC

		GC 415 T-10	92%	N/A	-42.8	5.0	N/A	HMC
		GC 415 T-11	86%	N/A	-40.6	4.9	N/A	HMC
		GC 415 T-12	86%	N/A	-41.0	4.9	N/A	HMC
		GC 415 T-13	86%	N/A	-33.1	4.9	N/A	HMC

N/A = not available

Cluster analysis using k-means method, applied on $\delta^{13}C_{CaCO3}$ and $\delta^{34}S_{CRS}$ data produced in this study and those from published reports, suggest an optimal k between 3 to 4, after which the cost function decreases by very small amounts with each iteration (Fig. 5). Visualization of data with the help of cluster analysis and site characteristics suggests four sample groups with distinctly different DIC and sulfide sourcing inferred from the paired $\delta^{13}C_{CaCO3}$ and $\delta^{34}S_{CRS}$ values:

(i) samples from methane seepage sites showing AOM as the dominant diagenetic process

(ii) samples from oil seepage sites that show AONM as a dominant process

(iii) samples from organoclastic sulfate reduction (OSR) dominated setting

(iv) samples showing a mixed sources for DIC and sulfide showing values intermediate between the other three end-members.

The decision boundaries of end-members were loosely defined based on cluster density and site characteristics (seep type, Table 1). While AOM and AONM end-members were clearly distinguishable, the boundary between AONM and OSR as well as OSR and mixed pool were less distinct. Section 5.4 discusses these results in detail.

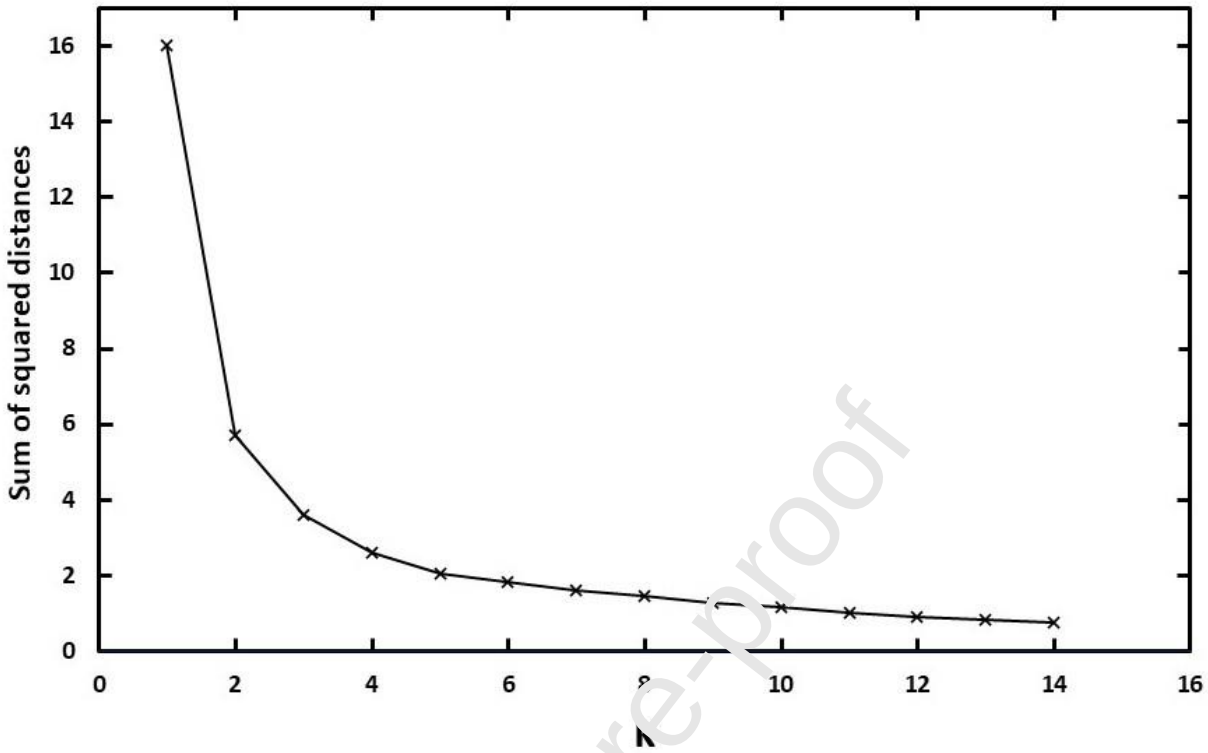

Figure 4: Optimum number of clusters determined by elbow method from unsupervised k-means learning algorithm on $\delta^{13}C_{CaCO3}$ and $\delta^{34}S_{CRS}$ data produced in this study and that from published data.

5. Discussion

Our results offer a broader evaluation of the sulfate reduction processes that contribute to the DIC pool for carbonate authigenesis on the GoM seafloor and their geochemical distinctions based on C-S isotopes. Seafloor and petrographic observations suggest multiple seepage events at Chapopote Knoll and that much of this biogeochemical activity occurs not only interstitially but also endolithically, where microbes inhabit the carbonate crust interiors. We were also able to produce the first U-Th based dates for authigenic carbonates from the southern GoM.

5.1 Petrographic Observations – Endolithic Biosignatures

Petrographic observations suggest precipitation of authigenic carbonate and sulfide minerals in a dynamic seep setting with episodic fluid flow, microbial activity, and associated cycling of C, S, and Fe (Figs. 2 and 5). Peloidal micrite exhibiting a clotted fabric (Fig. 2E) has been reported widely from seep carbonates and is indicative of early-stage cementation resulting from

microbial interactions (Cavagna et al., 1999; Peckmann et al., 2002; Flügel, 2004). Microbially oxidized crude oil coating aragonite crystals and pore spaces suggests a close association between carbonate authigenesis and hydrocarbon seepage from the subsurface. Abundant authigenic pyrite in the carbonate matrix (Fig. 2F) is suggestive of sulfate reduction coupled to anaerobic hydrocarbon oxidation, which increases carbonate alkalinity while generating dissolved sulfide, the latter forming pyrite through reaction with reactive Fe phases (Peckmann et al., 2001; Peckmann and Thiel, 2004).

Evidence for multiple seepage episodes include distinctly younger carbonate cementation around pore spaces and fractures through clasts (Fig. 2 and 5). We propose that fracture-filling carbonate cement is evidence for multiple seepage events as well as potential endolithic activity. It has been shown that seep carbonates can serve as a unique microbial habitat for endolithic activity capable of continued anerobic hydrocarbon oxidation and authigenic carbonate aggregation even after their formation (Marlow et al., 2014; Marlow et al., 2015; Yanagawa et al., 2019). Marlow et al. (2015) used the term 'autoendolithic' for such endolithic activity because that microbial metabolism induces mineral precipitation and leads to the formation of rock that remains inhabited by the same kind of microbes. We also observed pervasive fractures, potentially caused by *in situ* brecciation of semi-indurated sediments and clasts, resulting from pressure induced by rising hydrocarbons (e.g., Hovland et al., 1987; Beauchamp and Savard, 1992; Campbell et al., 2008). These features were subsequently filled by aragonitic seams and are commonly observed together with hydrocarbon inclusions. These may indicate episodic seepage and subsequent carbonate precipitation events via anaerobic hydrocarbon oxidation (Fig. 5A-E). Hence we propose that these fracture-filling signatures could be indicative of autoendolithic structures reflecting self-entombment of hydrocarbon-oxidizing microbes (Marlow et al., 2015, Fig. 5F). In addition, Campeche seep carbonates were shown to entrap methane and other hydrocarbons (C_2 up to C_6) in the crystal spaces of carbonate minerals (Blumenberg et al., 2018). The presence of trapped gases may trigger anaerobic hydrocarbon oxidation coupled with sulfate reduction (considering the aragonite crusts are formed near the sediment-water interface with high porosity, allowing sulfate diffusion), resulting in carbonate authigenesis and potentially endolithic activity. Future work using fluorescence microscopy along with high-resolution atomic force microscopy is expected to shed more light on these unique biosignatures.

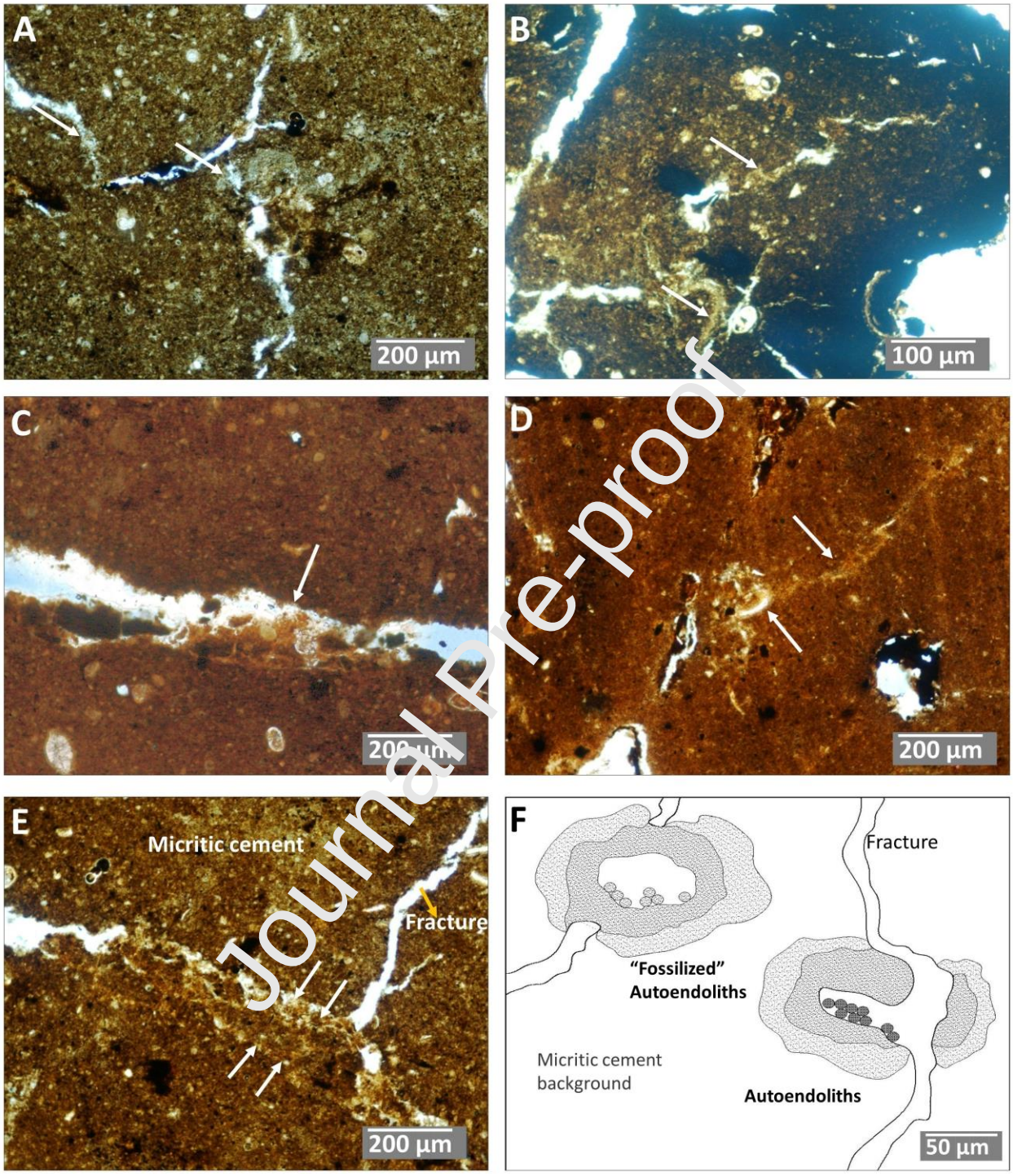

Figure 5: Evidence for common endolithic activity in fractures of micritic cements at Chapopote Seeps (A-E) and interpretative drawing of autoendolithic microbe-rock relationship (F). Hydrocarbon oxidation by the microbial communities inhabiting the fractures of the seep carbonates induce additional carbonate precipitation, leading to self-entombment of

hydrocarbon-oxidizing microbes (autoendolithic activity). White arrows mark sites of potential mineralization induced by autoendolithic activity and the yellow arrow in Figure E marks a fracture Figure F is a schematic representation for relative locations and microbe-rock interactions of autoendolithic organisms adapted from Marlow et al., 2015. Circles represents endoliths and gray shading represents successive zones of autoendolithic carbonate precipitation. Refer to section 5.1 for discussion.

5.2 Temporal Variability of GoM Seeps

Since authigenic carbonates may serve as a reliable geological archive for seepage histories including C and S cycling, constraining their precipitation ages should provide us a glimpse of the temporal patterns, causes, controls, and consequences of seep systems. U-Th dating of seep carbonates is a proven tool for constraining past seep activity at diverse seep settings globally (Aharon et al., 1997; Teichert et al., 2003; Watanabe et al., 2008; Bayon et al., 2009; Mazumdar et al., 2009; Liebetrau et al., 2010; Wirsig et al., 2016; Berndt et al., 2014; Crémière et al., 2016; Prouty et al., 2016; Mazzini et al., 2017; Sauer et al., 2017; Chen et al., 2019; Himmler et al., 2019; Judd et al., 2019; Wei et al., 2020).

To the best of our knowledge, our U-Th dates are the first for authigenic carbonates from the southern GoM. Only a few studies (Aharon et al., 1997; Feng et al., 2010) have reported U-Th dates for seep carbonates in the GoM. Also, Bian et al. (2013) constrained long-term seepage variability using ^{14}C dates on bivalve shell materials cemented in the seep carbonates. These studies were limited to the northern GoM, and so the timing and duration of seepage in the southern GoM is unknown. Sediment supply, sea-level changes, and salt deformation are suggested as the major factors that controlled recent hydrocarbon seeps in the GoM (Roberts and Carney, 1997).

Previous U-Th age-dates from northern GoM seeps along the lower continental margin and from upper bathyal depths to the abyssal plains showed strong evidence of discontinuous fluid flux in these basins during the late Quaternary (Aharon et al., 1997; Feng et al., 2010). Interestingly, the ages of many authigenic carbonate samples there clustered around 12 ka, suggestive of a role played by sediment loading and salt tectonics on glacial-interglacial time scales. Lower sea level would induce higher sediment loading on continental slopes. Rising sea level associated with deglaciation, in contrast, should reduce sediment loading in deeper waters by shifting deposition

landward to cause salt tectonic adjustment and the development of fault conduits for hydrocarbon seepage (Aharon et al., 1997; Feng et al., 2010; Roberts and Feng, 2013). Our age dates fall within that last deglaciation time frame, with the oldest being 13.5 ka and the youngest being 4.6 ka (BP).

While the northern GoM is dominated by sediment loading from the Mississippi river, southern GoM receives strong discharge from the Grijalva-Usumacinta River, the second largest river draining into the GoM following the Mississippi (Salas-de-León et al., 2008). The salt activity of the southern GoM is likely analogous to that of the Texas-Louisiana slope owing to its shared geological history (Garrison and Martin, 1973). Shallow sediment and salt structures associated with regional salt tectonics are shown to have dominant control on seep distribution along the Campeche Knolls (Ding et al., 2008; Ding et al., 2010). These factors suggest possible fault activation of hydrocarbon seepage linked to changes in sediment loading in the Campeche Bay during deglaciation, similar to the controls in the northern GoM (Feng et al., 2010; Roberts and Feng, 2013). A case for sediment-loading-driven salt tectonics as the cause for seep initiation in southern GoM, however, demands additional study. Nevertheless, our U-Th age data from the southern GoM combined with existing northern GoM data strongly suggest that seeps along GoM slopes were particularly active during the last deglaciation.

5.3 Carbon sources for DIC and $CaCO_3$

Based on the average $\delta^{13}C_{CaCO3}$ value of –25‰, a predominantly crude oil source for carbon was suggested for Chapopote seep carbonates (up to 90%) by Naehr et al. (2009). This inference was derived using carbon isotope mass balance based on the isotopic composition of end members including methane ($\delta^{13}C_{CH4}$ = –55‰ [MacDonald et al., 2004]), crude oil (average $\delta^{13}C$ value for GoM basin = –27‰ [Anderson et al., (1983]), sedimentary organic matter ($\delta^{13}C$ = –20‰ [Goñi et al., 1998]), and DIC from seawater ($\delta^{13}C$ = +1‰ [Aharon et al., 1991]). The headspace methane isotope measurement ($\delta^{13}C_{CH4}$ = –55‰) from Chapopote Knoll is indicative of a thermogenic ($\delta^{13}C_{CH4}$ range –30‰ to –50‰) and biogenic [$\delta^{13}C_{CH4}$ range –60‰ to –90‰] admixture (MacDonald et al., 2004; Naehr et al., 2009). Measured $\delta^{18}O_{CaCO3}$ values ranged from +3.3 to +5.9 ‰, averaging +4.5‰. This was higher than the calculated $\delta^{18}O_{CaCO3}$ value (+3.02‰) based on the measured bottom water temperature (4.02°C) and pore fluid $\delta^{18}O$ values (+0.09‰) of background samples, according to Kim et al. (2007) (Supp. Table 2). Porewater ^{18}O-

enrichment sourced from shallow gas hydrate dissociation could explain this difference (Davidson et al., 1983; Naehr et al., 2009). These observations agree with Formolo et al. (2004), who suggested that $\delta^{13}C$ of DIC (and $CaCO_3$) at oil seep settings such as our study site may be swamped by AONM signals despite the presence of shallow pockets of gas hydrates, while the $\delta^{18}O$ signals of adjacent porewater ($CaCO_3$) are isotopically sensitive to ^{18}O-enrichment from shallow hydrate dissociation.

5.3.1 Crude oil oxidation (AONM)

Multiple lines of evidence point to crude oil oxidation coupled with sulfate reduction as the dominant DIC source for carbonate precipitation of Chapopote Knoll.

(1) the $\delta^{13}C_{CaCO3}$ values averaging –25‰ are closer to a crude oil signature;
(2) the presence of abundant biodegraded crude oil within the carbonate samples (Fig. 2);
(3) widespread crude oil degradation signals from organic geochemistry studies on asphalts, oily sediments, and seeping crude oil (Schubotz et al., 2011b);
(4) an abundant unresolved complex organic mixture (UCM) in the carbonate pore-filling crude oil (Naehr et al., 2009), with an elevated baseline for the C15 to C30 range indicative of degradation involving loss of labile n-alkanes and isoprenoids from crude oil (Mansour and Sassen, 2011; Schubotz et al., 2011b);
(5) recently reported evidence from Chapopote seep sediments for a symbiotic microbial consortium composed of short-chain alkanes degraders with contributions from sulfate-reducing bacteria (Laso-Pérez et al., 2019);
(6) distinctive phase-specific enrichment of rare earth elements and U in Chapopote carbonates compared to methane-derived carbonates (Smrzka et al., 2016); and
(7) geochemical batch modeling suggestive of sulfate-driven crude oil oxidation contributing to carbonate precipitation at Campeche Knolls (Smrzka et al., 2019).

These multiple lines of evidence developed over the past two decades at Campeche Knolls, along with our petrographic observations and $\delta^{13}C_{CaCO3}$ data, allow us to use Chapopote seep carbonates as a template for recognizing authigenic carbonates sourced via AONM in other regions.

5.4 C-S Isotope Systematics of the AOM and AONM settings

To test the veracity of AONM signals at Campeche Knolls, we also analyzed sediments from GC 415 and GC 185 and gathered published data from multiple seep settings in the GoM (Formolo and Lyons, 2013; Feng et al., 2016; Sun et al., 2020). This extensive database allowed us to compare and contrast the C-S isotope systematics of sulfide and DIC produced via sulfate driven AOM and AONM as recorded in GoM seep $CaCO_3$ (Table 2 and Supp. Table 1). Along with the help of cluster analysis and site characteristics, we were able to define two dominant end members based on $\delta^{13}C_{CaCO3}$ versus $\delta^{34}S_{CRS}$ plots (Fig. 6):

(1) AOM-dominant seepage sites with strong ^{13}C-depletion in $CaCO_3$ ($\delta^{13}C_{CaCO3} < -40‰$) indicating a methane source for carbon; and $^{34}S_{CRS}$ values with ^{34}S-enrichment ($\delta^{34}S_{CRS} >0‰$) suggestive of dissolved sulfide production and sulfide mineral precipitation associated with AOM (e.g., Jørgensen et al., 2004; Borowski et al., 2013);

(2) Crude oil oxidation sites dominated by AONM as expressed in moderate ^{13}C-depletion in $\delta^{13}C_{CaCO3}$ ($\delta^{13}C_{CaCO3} = -25.8‰ \pm 1.5$) and $\delta^{34}S_{CRS}$ values with relatively strong ^{34}S-depletion ($\delta^{34}S_{CRS} < -15‰$), suggesting DIC sourced from AONM. These samples include virtually all (98%) of the Chapopote seep carbonates in this study and those from northern GoM sites GC 185 and GC 232, crude oil seep sites (Feng et al., 2009; Sun et al., 2020).

The data points lying between the two end members indicate mixing from multiple carbon sources and biogeochemical processes (DIC and sulfide pools from AOM, AONM, sedimentary organic matter degradation, DIC sourced from methanogenesis and the water column, as well as likely δ^{34}S signals from secondary sulfur cycling (e.g., Raiswell, 1987; Naehr et al., 2000; Formolo and Lyons, 2013; Crémière et al., 2020). Overall, as explained below, we seem able to identify sources of carbon for the DIC pool and suggest the particular sulfate reduction pathway that generates DIC and dissolved sulfide, namely AOM, AONM, or OSR. This observation also agrees with previously observed disparities between measured rates of sulfate reduction and methane oxidation (Joye et al., 2004; Bowles et al., 2011). Those data suggest that sulfate reduction is not driven primarily by AOM—thus highlighting the complex C-S relationship, with sulfate reduction coupled to both AOM and AONM at GoM seeps.

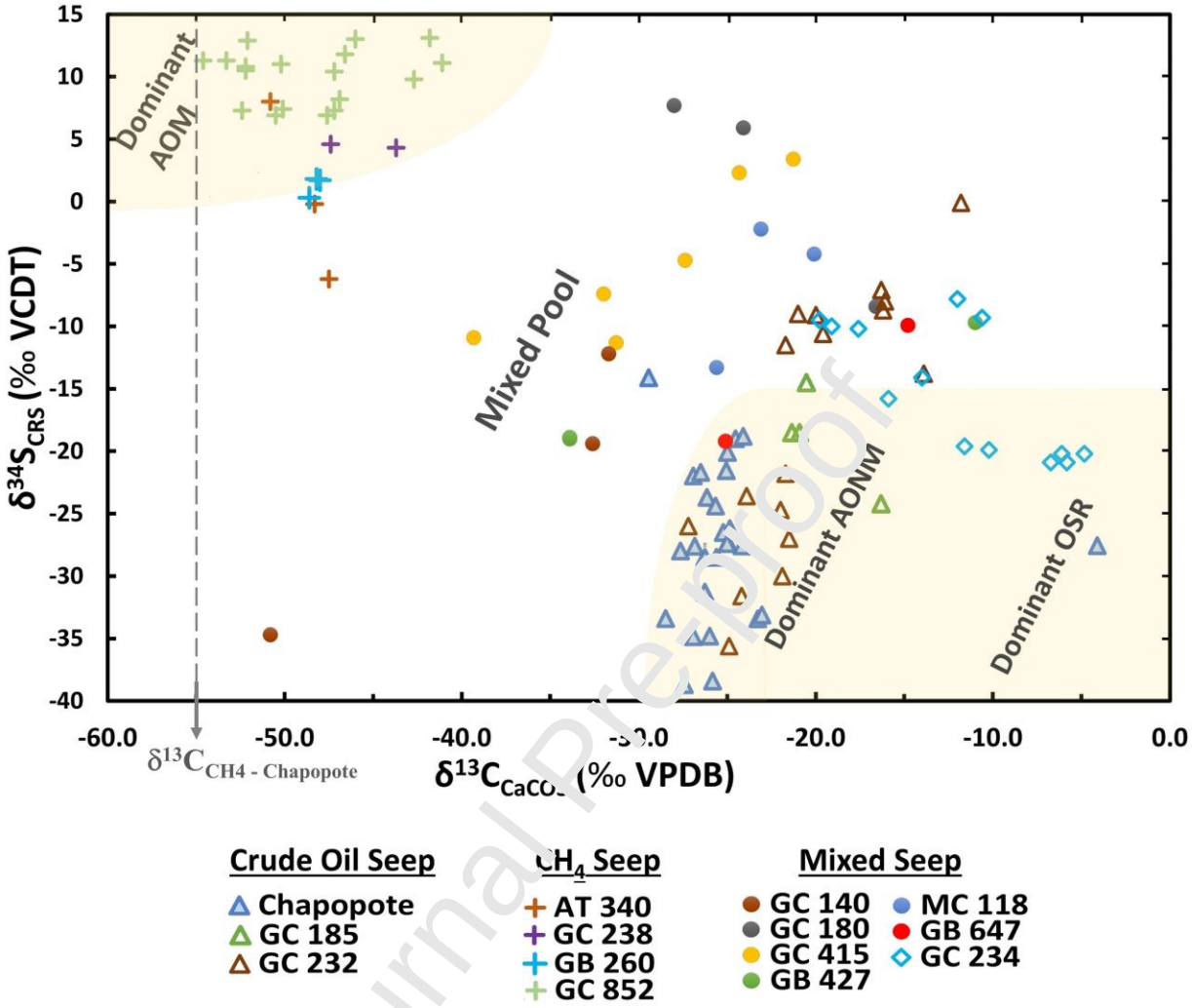

Figure. 6: Cross plot of $\delta^{13}C_{CaCO3}$ vs. $\delta^{34}S_{CRS}$ values from authigenic calcium carbonate (CaCO3) and selected shell samples found within surface sediments at various seep sites in the Gulf of Mexico. We sampled sediment at Chapopote Knoll (blue triangles) and measured isotopic values of sediments from GC 185 and GC 415. Other data are taken from the literature. Symbols refer to different types of seepage: sites with dominant oil seepage are represented by crosses (Chapopote Knoll, GC 232, and GC 185), sites with dominant methane seepage are shown with triangles (AT 340, GB 260, GC 238, and GC 852), and remaining sites with a mixture of oil and methane seepage are shown with circles. Vertical dashed line shows the $\delta^{13}C_{CH4}$ value for Chapopote headspace methane samples. The decision boundaries (shaded areas) of end-members were loosely defined based on the cluster density and site characteristics. Refer to Table 1 for site descriptions, Supp. Table 1 for data, and section 5.4 for discussion.

The $\delta^{13}C_{DIC}$ signatures for AOM and AONM varies primarily because the $\delta^{13}C$ of the substrates – CH_4 vs oil – are very different (section 5.3) and this affect the carbon isotopic composition of the DIC pool markedly (Formolo et al., 2004; Naehr et al., 2009; Mansour and Sassen, 2011; Roberts and Feng, 2013). However, the possibility of multiple carbon sources (section 5.3; e.g., methane, crude oil, seawater DIC, sedimentary organic matter) and associated processes (AOM, AONM, OSR, methanogenesis) leading to varying degrees of carbon-isotope fractionations of DIC at seeps (Sassen et al., 2004; Meister et al., 2019) can limit the application of $\delta^{13}C_{CaCO3}$ as a single proxy to evaluate the DIC sourcing at seeps. Hence, we highlight that the combination of paired $\delta^{13}C_{CaCO3}$ and $\delta^{34}S_{CRS}$ offers additional constraints to distinguish the DIC and sulfide sourcing through sulfate reduction coupled to the oxidation of different carbon substrates (mainly methane vs crude oil).

The $\Delta^{34}S_{sulfate–sulfide}$ ($\delta^{34}S_{seawater\ sulfate} - \delta^{34}S_{porewater\ sulfide}$) depends on the rate at which seawater sulfate exchanges with subsurface diagenetic horizons and the isotopic fractionation by sulfate-reducing microbes (Kaplan and Rittenberg, 1964; Habicht and Canfield, 1997; Wehrmann et al., 2011; Kump, 2012; Fike et al., 2015). In a comparative study of sulfate reduction rates from a gas seep, oil seep, and non-seep background sites in GoM, Aharon and Fu (2000) reported highest sulfate reduction rates at methane seep (0.27 to 2.51 µm SO_4^{2} cm^{-3} day^{-1}) followed by oil seep (0.01 to 0.22 µm SO_4^{2-} cm^{-3} day^{-1}) and non-seep background sediments (0.0043 µm SO_4^{2-} cm^{-3} day^{-1}). These results suggests that the carbon substrate undergoing oxidation coupled to sulfate reduction has an important control on the sulfate reduction rates and associated isotope fractionations that can impact the $\delta^{34}S_{sulfide}$ value (Aharon and Fu, 2000; Sun et al., 2020).

In a typical marine setting lacking significant methane transport, OSR would predominate. In such settings, slow sulfate reduction rates lead to high fractionations, which, under non-limiting sulfate conditions (open-system), would result in low $\delta^{34}S_{sulfide}$ values (Jorgensen, 1979; Canfield, 2001; Lin et al., 2017b). In contrast, sites with higher subsurface methane fluxes often show higher rates of sulfate reduction due to AOM and exhaustion of sulfate in the local sulfate pool (closed-system) within the sediment column, resulting in high rates of sulfide mineral precipitation around the SMTZ with enriched ^{34}S signals (Peckmann et al., 2001; Jørgensen et al., 2004; Wang et al., 2008; Lim et al., 2011; Peketi et al., 2012; Borowski et al., 2013; Deusner et al., 2014; Peketi et al., 2015; Li et al., 2016; Lin et al., 2016a; Lin et al., 2016b; Li et al., 2017;

Lin et al., 2017a; Fan et al., 2018; Wu et al., 2019; Argentino et al., 2020). Provided sufficient Fe availability to form iron sulfide minerals, $\delta^{34}S_{CRS}$ would be a good recorder for the porewater sulfide since isotopic fractionation associated with the sulfide mineral formation from dissolved sulfide is negligible (Price and Shieh, 1979; Butler et al., 2004). In addition to the closed-system behavior, the enriched $\delta^{34}S_{CRS}$ signals we observe at methane seep sites are also suggestive of small instantaneous fractionations associated with rapid rates of sulfate reduction resulting in isotopically heavy sulfide that gets captured by available Fe early in the process close to the sediment-water interface (E.g., Kaplan and Rittenberg, 1964; Chanton, 1985; Lyons, 1992; Lyons, 1997; Gilhooly et al., 2016).

Oil seepage settings, where AONM occurs, could result in sulfate reduction rates higher than those associated with OSR but lower than AOM (Aharon and Fu, 2000; Aharon and Fu, 2003). Thus, AONM yields fractionations larger than those associated with AOM as well as less efficient removal of sulfate. The net result would be relatively depleted ^{34}S signals in sulfide minerals. Some of the variability within the observed low $\delta^{34}S_{CRS}$ values (–10 to –39‰) can be attributed to the diversity and concentration of hydrocarbon compounds involved and related differences in sulfate reduction rates, microbial species and metabolic diversity, as well as varying impacts of secondary sulfide cycling such as sulfide oxidation and disproportionation (Kemp and Thode, 1968; Canfield and Thamdrup, 1994; Detmers et al., 2001; Habicht and Canfield, 2001; Lyons and Gill, 2010; Sim et al., 2011; Gallagher et al., 2012; Leavitt et al., 2013; Deusner et al., 2014; Colangelo-Lillis et al., 2019; Jørgensen et al., 2019; Pellerin et al., 2019; Bazzaro et al., 2020; Crémière et al., 2020). Overall, however, highly negative $^{34}S_{CRS}$ cluster ($\delta^{34}S_{CRS}$ < –15‰) linked to AONM seem distinct from the dominantly heavier isotopic cluster associate with AOM. It is also noteworthy that $\delta^{13}C_{CaCO3}$ and $\delta^{34}S_{CRS}$ values for Chapopote Knoll, GC 232, and GC 185—the three sites with oil seepage and AONM—show similar $\delta^{13}C$ and $\delta^{34}S$ signals (Fig. 6). Hence, we interpret the high $\delta^{34}S_{sulfide}$ and very low $\delta^{13}C_{DIC}$ values in our compilation to be sourced predominantly by AOM and the relatively low $\delta^{34}S_{sulfide}$ and moderately low $\delta^{13}C_{DIC}$ values to be sourced primarily from crude oil oxidation and OSR (Fig. 6).

The aragonitic composition of Chapopote carbonates is strongly supportive of a shallow diagenetic origin in the presence of sulfate, low phosphate concentration, and high Mg/Ca ratios

(Burton and Walter, 1990; Burton, 1993). Aloisi et al. (2002) suggested that porewater sulfate concentration can play an important role in determining seep carbonate mineralogy since sulfate inhibits Mg-calcite precipitation and favors aragonite formation. Alternatively, Mg-calcite precipitation maybe catalyzed by the presence of sulfide ions, which accelerate Mg dehydration and incorporation into the mineral lattice (Zhang et al., 2012; Zhang et al., 2013; Lu et al., 2018; Smrzka et al., 2021). Mansour (2014), in a compilation based on seep carbonates from multiple GoM sites, suggested that aragonite is the dominant mineralogy at sites of crude oil oxidation in comparison to methane seep settings due to relatively lower sulfate reduction rates during crude oil oxidation. This relationship was also reported for crude oil oxidation at site GC 185 by Feng et al., (2009) and GC 232 by Sun et al. (2020). Aragonite mineralogy of authigenic carbonates reported from Chapopote corroborate to these findings (Fig. 7). AOM-dominated samples, in contrast, showed a diverse mix of carbonate compositions spanning aragonite, high-Mg calcite, and low-Mg calcite (Fig. 7). Sufficient Fe availability for iron sulfide mineral precipitation is necessary when considering $\delta^{34}S_{CRS}$ as a faithful recorder of porewater sulfate reduction processes, which is not always the case in many GoM seep settings, especially below the surface-most sediment layers (Formolo and Lyons, 2013). Hence aragonite samples, preferably formed closer to the sediment-water interface (e.g., Feng et al., 2016), where high interstitial sulfide concentrations and sufficient Fe availability are more likely, serves ideal targets to evaluate the AOM versus AONM distinction based on $\delta^{13}C_{CaCO3}$ and $\delta^{34}S_{CRS}$.

While the AOM and AONM signals were clearly distinguishable, the boundary between crude oil oxidation and OSR is not clearly defined based on existing data. The $\delta^{34}S_{CRS}$ data fail to show a clear distinction between OSR and AONM (Fig. 6). The $\delta^{13}C_{CaCO3}$ results also do not clearly demarcate the two processes likely due to combination of similar values between $\delta^{13}C$ values of organic matter and oil, slight fractionation between organic matter and DIC, and mixing of DIC sources. This challenge is exacerbated by the fact that our samples and most of the literature data compiled considered here are from seep sites. For example, data from site GC 234 taken from Formolo and Lyons (2013), despite belonging to a seep site, plot with the OSR cluster, with only a hint of seep-induced C-S signals (average $\delta^{13}C_{CaCO3}$ = -11.9‰ and $\delta^{34}S_{CRS}$ = -15.3‰). This contradiction comes as no surprise because the data likely reflect a combination of OSR, AONM, and Fe-limitation (Formolo and Lyons, 2013)—pointing to the need for additional paired

$\delta^{13}C_{DIC}$-$\delta^{34}S_{sulfide}$ data from both OSR and seep-dominant sites from the GoM to better constrain the end members as well as the frequent cases of mixed signals.

There are a few additional arguments that lend support to the possibility of distinguishing between OSR and AONM in our cross plot. The carbonate content for the samples that plot in OSR cluster is very low (e.g., average carbonate content ~24% Supp Table. 1) in comparison to the crude oil seep samples (average carbonate content = ~80%). This observation is in agreement with reports suggesting that authigenic carbonate precipitation decreases at low sulfate reduction rates, due to the dominant effect of H^+ over bicarbonate (Meister, 2013; Zhang, 2020). Further, samples in the OSR cluster show minimal ^{18}O-enrichment (Fig. 3C, Supp. Table 1), unlike a seep-dominant AONM setting where the $\delta^{18}O_{CaCO3}$ signals are often influenced by ^{18}O enrichment sourcing from localized shallow gas hydrate dissociation (Formolo et al., 2004), deep hydrocarbon rich brines (Mansour and Sassen, 2011), and (less likely) clay mineral dehydration (Roberts and Feng, 2013). These observations, along with enriched $\delta^{13}C_{CaCO3}$ values than AONM samples, suggest that the data from GC 234 plotting in the OSR cluster are likely influenced more by OSR than AONM.

Recent studies have shown that multiple sulfur isotope signatures of sulfide minerals ($\Delta^{33}S$ and $\delta^{34}S$) could be an effective tool to distinguish between OSR and AOM (Lin et al., 2017b; Gong et al., 2018; Lin et al., 2018; Crémière et al., 2020; Liu et al., 2020). Such efforts, along with incorporation of new data from additional seep and OSR dominant sites, will improve the definition of end-member boundaries. The relative roles of aerobic and anaerobic pathways of hydrocarbon oxidation in surface/near-surface sediments also remain fodder for future research as related to carbonate precipitation and dissolution (Aller, 2014). Redox-sensitive proxies such rare earth element patterns and biomarker records of aerobic hydrocarbon oxidizers preserved in the carbonate matrix will aid in these distinctions (Feng et al., 2009; Birgel et al., 2011; Smrzka et al., 2020)

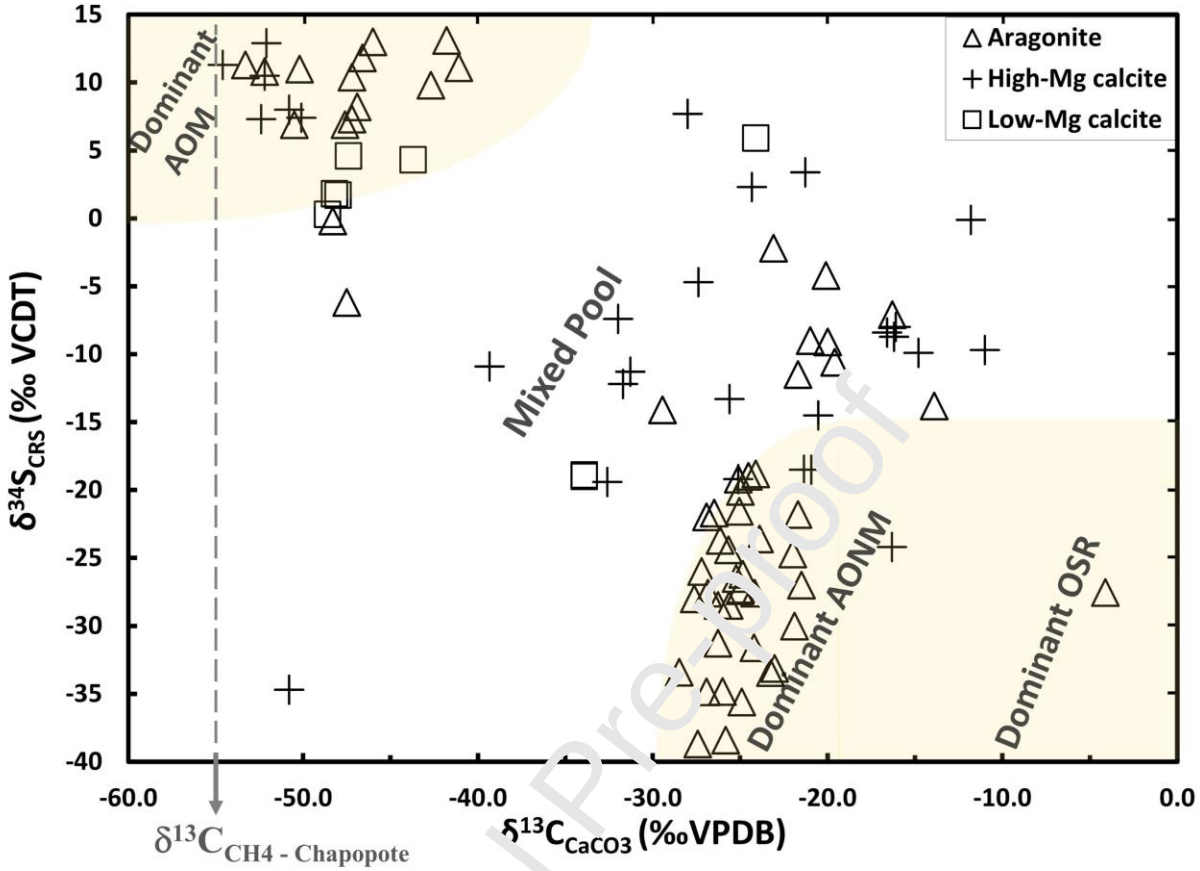

Figure 7: Cross plot of $\delta^{13}C_{CaCO_3}$ vs. $\delta^{34}S_{CRS}$ values of various phases of authigenic calcium carbonate ($CaCO_3$) and selected shell samples as aragonite (triangles), and low-Mg and high-Mg calcite (squares and crosses, respectively), and of authigenic pyrite found within surface sediments of oil seep sites, Chapopote Knoll, Gulf of Mexico; and Northern GoM seep sites plotted in Fig. 6. GC 234 did not have the mineralogy information hence is not included in the plot. Vertical dashed line shows the $\delta^{13}C_{CH4}$ value for Chapopote headspace methane samples. The shaded areas on the top left and bottom right represent the same AOM and AONM+OSR endmember pools in Fig. 6.

5.5 Implications for the sedimentary record

Carbonate systems are Earth's largest carbon reservoir, accounting for >60 million Gt C (Falkowski et al., 2000). Carbonate burial in marine sediments is an important part of carbon cycling through most of the geological history, accounting for ~80% of the total carbon removal

from Earth's surface today (Derry, 2014; Sun and Turchyn, 2014; Berg, 2018). $\delta^{13}C_{CaCO3}$ signals from the geologic record are an important sedimentary proxy in efforts to understand the evolution of the carbon cycle and the chemical composition of the ocean-atmosphere system over geological history (Hayes et al., 1999; Berner, 2003; Katz et al., 2005). For example, a period of higher organic carbon burial would remove more ^{12}C carbon, resulting in ^{13}C-enrichment in DIC (and $CaCO_3$) (Berner, 2003; Canfield and Kump, 2013; Lyons et al., 2014). This approach has been used to reconstruct organic carbon burial and the oxygen content of the atmosphere (Shackleton, 1985; Kump and Arthur, 1999; Berner, 2004). Authigenic carbonate precipitation was invoked as a third major carbon sink, with major impact on $\delta^{13}C_{CaCO3}$ fluctuations in the geological record (Schrag et al., 2013). Further, authigenic carbonate precipitation may result in significant carbon sequestration at present, comparable to ~15% of carbonate accumulation on continental shelves and in the abyssal ocean, respectively (Akam et al., 2020). Hence, better characterization of the sedimentary proxies for authigenic carbonate formation is an important goal (e.g., Bjerrum and Canfield, 2011; Bristow and Grotzinger, 2013; Zhao et al., 2016; Cui et al., 2017; Davis Barnes et al., 2019; Jiang et al., 2019).

Our results emphasize an important additional process for C-S coupling through organic carbon decomposition and resulting authigenic carbonate formation—crude oil oxidation (Formolo et al., 2004; Peckmann et al., 2007; Naehr et al., 2009; Mansour and Sassen, 2011; Formolo and Lyons, 2013; Kiel and Peckmann, 2019; Smrzka et al., 2019)—to add to the well-known processes of AOM and OSR (Bradbury and Turchyn, 2019; Akam et al., 2020). Further, we explore the use of cross-plotting $\delta^{13}C_{CaCO3}$ versus $\delta^{34}S_{CRS}$ to distinguish crude oil seepage and methane seepage processes in present sediments and in the geologic record, which can be confirmed using additional evidence, such as petrography and mineralogy (Mansour, 2014), biomarker analysis (particularly unresolved complex mixture suggestive of petroleum degradation; Sassen et al., 2001; Naehr et al., 2009; Mansour and Sassen, 2011), trace metal and rare earth element concentration (Smrzka et al., 2016; Smrzka et al., 2019), and total organic carbon and total organic sulfur contents (Sun et al., 2020). Our $\delta^{13}C_{CaCO3}$ versus $\delta^{34}S_{CRS}$ from GoM could serve as a template for assessment of carbon sources and sulfate-reduction and other early diagenetic processes from additional sites and regions. Further, authigenic carbonate records have been used to estimate past methane fluxes (e.g., the Neoproterozoic caprocks of Snowball Earth; Kennedy et al., 2001; Jiang et al., 2003). An ability to better distinguish

methane-driven carbonate authigenesis from that derived from oxidation of other hydrocarbons could allow us to better constrain the temporal variations in methane fluxes over geologic history.

6. Conclusion

We examined the C-S coupling and temporal patterns for Chapopote asphalt seeps in the southern Gulf of Mexico based on $CaCO_3$ geochemistry and compared our result with data available from multiple northern GoM seep sites. Carbonate petrography of Chapopote samples showed peloidal textures and autoendolithic features, indicative of a dynamic, microbially-driven biogeochemical process resulting in carbonate authigenesis. We present the first U-Th-based ages for seep carbonates from the southern GoM. U-Th ages for Chapopote seep carbonates ranged from 13.5 ka to 4.6 ka (BP), suggesting that Chapopote asphalt seepage has been ongoing for thousands of years. These results encourage further investigation that GoM slopes might have experienced seep activation during the last deglaciation owing to changes in sedimentary loading and associated salt-tectonic adjustment, which activates fault conduits for deep-seated hydrocarbon seepage.

Isotopic measurements of the authigenic minerals of calcium carbonate ($CaCO_3$) and bulk sulfide minerals (native sulfur, iron monosulfides, pyrite) reveal the geochemical characteristics of interstitial DIC and dissolved sulfide. A cross plot of $\delta^{13}C_{CaCO3}$ and $\delta^{34}S_{CRS}$ distinguishes between carbon substrates (methane vs. crude oil) and between the sulfate-reduction processes of anaerobic oxidation of methane (AOM) and anaerobic oxidation of non-methane (AONM).. Authigenic carbonate samples from asphalt seeps at Chapopote Knolls showed distinct signatures, with $\delta^{13}C_{CaCO3}$ and $\delta^{34}S_{CRS}$ values characterized by moderate ^{13}C-depletions ($\delta^{13}C_{CaCO3} \sim -25‰$) and relatively strong ^{34}S-depletions ($\delta^{34}S_{CRS} < -15‰$), indicative of DIC sourcing via AONM. AOM-dominant seepage sites, in contrast, show strong ^{13}C-depletion in $CaCO_3$ ($\delta^{13}C_{CaCO3} < -40‰$) and noticeable ^{34}S-enrichment in sulfide minerals ($\delta^{34}S_{CRS} > 0‰$) values, indicative of predominantly AOM sourcing for DIC. The spread of data in between the two end-members indicate mixing from multiple sources (DIC and sulfide pools from AOM, crude oil oxidation, organic matter degradation, secondary sulfide cycling, as well as DIC sourced from methanogenesis and the water column). Future work on triple S isotopes, organic S, and CAS may shed light on the full extent of sulfur cycling in these settings as well as to

improve the current field boundaries. $\delta^{13}C_{CaCO3}$ versus $\delta^{34}S_{CRS}$ compilation from the GoM could serve as a template for data from additional sites and regions and highlights the importance for producing more paired $\delta^{13}C_{CaCO3}$ and $\delta^{34}S_{CRS}$ dataset from diverse seep and OSR dominated settings to build on this template. Overall, the combination of age-dating and detailed geochemical analyses highlights the potential for better evaluation of carbonate authigenesis in seep settings, which is a significant component of marine carbon burial and an important geological archive for seepage events.

Acknowledgments

SA would like to acknowledge the Graduate Research Grants from the American Association of Petroleum Geologists (AAPG), Geological Society of America (GSA), and Gulf Coast Association of Geological Societies (GCAGS). Scholarships to SA from TAMUCC Endowment Fund, Gulf Coast Chapter of Air & Waste Management Association (A&WMA), and Corpus Christi Geological Society (CCGS) are acknowledged for the support during this research. The Petroleum Research Fund of the American Chemical Society provided support to TWL. Christine Chen, Ben Hardt, and Gabriela Serrato Marks at McGee Lab (MIT) are thanked for the assistance during the U-Th analysis. The Lyons' group at UCR is acknowledged for the support to SA during the lab visit for isotope analysis. Pankaj Khanna, Tarini Bhatnagar, Wasif Riza, and Mustafa Kalam are thanked for their assistance with Figure 1 and cluster analysis. Samples for this study were obtained during *R/V SONNE* and *R/V Meteor* cruises SO174/2 and M67/2. We would like to extend our thanks to the entire team involved in those expeditions. We would like to thank Walter S. Borowski and an anonymous reviewer for the constructive inputs that greatly helped in improving this manuscript.

Declaration of Interest Statement

We declare that this manuscript entitled "Carbon-sulfur signals of methane versus crude oil diagenetic decomposition and U-Th age relationships for authigenic carbonates from asphalt seeps, southern Gulf of Mexico" with authors Sajjad A Akam, Timothy W. Lyons, Richard B.

Coffin, David McGee, Thomas H. Naehr, Steven M. Bates, Clay Clarkson, and Brandi Kiel Reese is original, has not been published before and is not currently being considered for publication elsewhere. We know of no conflicts of interest associated with this publication, and there has been no significant financial support for this work that could have influenced its outcome. As the corresponding author, I confirm this on behalf of all the named authors.

References

Aharon, P., 2000. Microbial processes and products fueled by hydrocarbons at submarine seeps, Microbial sediments. Springer, pp. 270-281.

Aharon, P., Fu, B., 2000. Microbial sulfate reduction rates and sulfur and oxygen isotope fractionations at oil and gas seeps in deepwater Gulf of Mexico. Geochimica et Cosmochimica Acta, 64(2): 233-246.

Aharon, P., Fu, B., 2003. Sulfur and oxygen isotopes of coeval sulfate–sulfide in pore fluids of cold seep sediments with sharp redox gradients. Chemical Geology, 195(1): 201-218.

Aharon, P., Graber, E.R., Roberts, H.H., 1991. Detection of hydrocarbon venting on the Gulf of Mexico sea floor from determinations of dissolved inorganic carbon and 13C of the water column overlying seeps. Gulf Coast Association of Geological Societies Transactions, 41: 2-9.

Aharon, P., Schwarcz, H.P., Roberts, H.H., 1997. Radiometric dating of submarine hydrocarbon seeps in the Gulf of Mexico. Geological Society of America Bulletin, 109(5): 568-579.

Akam, S.A., Coffin, R.B., Abdulla, H.A.N., Lyons, T.W., 2020. Dissolved Inorganic Carbon Pump in Methane-Charged Shallow Marine Sediments: State of the Art and New Model Perspectives. Frontiers in Marine Science, 7(206).

Akam, S.A., Coffin, R.B., Lyons, T., Bates, S.M., Reese, B.K., Clarkson, C.C., 2019. Reconstructing the Carbon-Sulfur Geochemistry of Hydrocarbon Seeps at the Gulf of Mexico from Authigenic Carbonates, AGU Fall Meeting 2019. AGU.

Aller, R.C., 2014. 8.11 - Sedimentary Diagenesis, Depositional Environments, and Benthic Fluxes. In: Holland, H.D., Turekian, K.K. (Eds.), Treatise on Geochemistry (Second Edition). Elsevier, Oxford, pp. 293-334.

Aloisi, G., Bouloubassi, I., Heijs, S.K., Pancost, R.D., Pierre, C., Sinninghe Damsté, J.S., . . . Rouchy, J.-M., 2002. CH4-consuming microorganisms and the formation of carbonate crusts at cold seeps. Earth and Planetary Science Letters, 203(1): 195-203.

Andersen, M., Stirling, C., Zimmermann, B., Halliday, A., 2010. Precise determination of the open ocean 234U/238U composition. Geochemistry, Geophysics, Geosystems, 11(12).

Anderson, R.K., Scalan, R.S., Parker, P.L., Behrens, E.W., 1983. Seep Oil and Gas in Gulf of Mexico Slope Sediment. Science, 222(4624): 619.

Argentino, C., Johnson, J., Conti, S., Fioroni, C., Fontana, D., 2020. Preservation of 34 S-enriched sulfides in fossil sulfate-methane transition zones: new evidence from Miocene outcrops of the northern Apennines (Italy). Geo-Marine Letters: 1-12.

Baker, P.A., Burns, S.J., 1985. Occurrence and formation of dolomite in organic-rich continental margin sediments. AAPG Bulletin, 69(11): 1917-1930.

Bayon, G., Henderson, G., Bohn, M., 2009. U–Th stratigraphy of a cold seep carbonate crust. Chemical Geology, 260(1): 47-56.

Bazzaro, M., Ogrinc, N., Relitti, F., Lucchi, R.G., Giani, M., Adami, G., . . . De Vittor, C., 2020. Geochemical signatures of intense episodic anaerobic oxidation of methane in near-surface sediments of a recently discovered cold seep (Kveithola trough, NW Barents Sea). Marine Geology: 106189.

Beauchamp, B., Savard, M., 1992. Cretaceous Chemosynthetic Carbonate Mounds in the Canadian Arctic. PALAIOS, 7(4): 434-450.

Berg, R.D., 2018. Quantifying the deep: The importance of diagenetic reactions to marine geochemical cycles.

Berndt, C., Feseker, T., Treude, T., Krastel, S., Liebetrau, V., Niemann, H., . . . Ferré, B., 2014. Temporal constraints on hydrate-controlled methane seepage off Svalbard. Science, 343(6168): 284-287.

Berner, R.A., 2003. The long-term carbon cycle, fossil fuels and atmospheric composition. Nature, 426(6964): 323-326.

Berner, R.A., 2004. The Phanerozoic Carbon Cycle : Co2 and O2. Oxford University Press, Incorporated, Cary, UNITED STATES.

Bian, Y., Feng, D., Roberts, H.H., Chen, D., 2013. Tracing the evolution of seep fluids from authigenic carbonates: Green Canyon, northern Gulf of Mexico. Marine and Petroleum geology, 44: 71-81.

Birgel, D., Feng, D., Roberts, H.H., Peckmann, J., 2011. Changing redox conditions at cold seeps as revealed by authigenic carbonates from Alaminos Canyon, Northern Gulf of Mexico. Chemical Geology, 285(1): 82-96.

Bjerrum, C.J., Canfield, D.E., 2011. Towards a quantitative understanding of the late Neoproterozoic carbon cycle. Proceedings of the National Academy of Sciences, 108(14): 5542-5547.

Blumenberg, M., Pape, T., Seifert, R., Bohrmann, G., Schlömer, S., 2018. Can hydrocarbons entrapped in seep carbonates serve as gas geochemistry recorder? Geo-Marine Letters, 38(2): 121-129.

Boetius, A., Ravenschlag, K., Schubert, C.J., Rickert, D., Widdel, F., Gieseke, A., . . . Pfannkuche, O., 2000. A marine microbial consortium apparently mediating anaerobic oxidation of methane. Nature, 407(6804): 623-626.

Bohrmann, G., 2008. Fluid Seepage in the Southern Gulf of Mexico (Campeche Bay): M67, Leg 2a, Cristobal-Tampico, 14 March-31 March, 2006: M67, Leg 2b, Tampico-Bridgetown, 3 April-25 April, 2006. Fachbereich Geowissenschaften, Universität Bremen.

Bohrmann, G., 2014. Asphalt Volcanism. In: Harff, J., Meschede, M., Petersen, S., Thiede, J. (Eds.), Encyclopedia of Marine Geosciences. Springer Netherlands, Dordrecht, pp. 1-3.

Bohrmann, G., Schenck, S., 2004. R/V SONNE cruise report SO174, OTEGA II, Balboa− Corpus Christi− Miami (1 October− 12 November, 2003). GEOMAR report, 117: 130.

Bohrmann, G., Spiess, V., B. Böckel, A. Boetius, M. Boles, M. Brüning, . . . Zabel, M., 2008. Report and preliminary results of R/V Meteor Cruise M67/2a and 2b, Balboa-Tampico-Bridgetwon, 15 March-24 April, 2006. Fuid seepage in the Gulf of Mexico. Department of Geosciences, Bremen University.

Borowski, W.S., Rodriguez, N.M., Paull, C.K., Ussler, W., 2013. Are 34 S-enriched authigenic sulfide minerals a proxy for elevated methane flux and gas hydrates in the geologic record? Marine and Petroleum Geology, 43: 381-395.

Bowles, M.W., Samarkin, V.A., Bowles, K.M., Joye, S.B., 2011. Weak coupling between sulfate reduction and the anaerobic oxidation of methane in methane-rich seafloor sediments during ex situ incubation. Geochimica et Cosmochimica Acta, 75(2): 500-519.

Bradbury, H.J., Turchyn, A.V., 2019. Reevaluating the carbon sink due to sedimentary carbonate formation in modern marine sediments. Earth and Planetary Science Letters, 519: 40-49.

Bristow, T.F., Grotzinger, J.P., 2013. Sulfate availability and the geological record of cold-seep deposits. Geology, 41(7): 811-814.

Brooks, J.M., Wiesenburg, D.A., Roberts, H., Carney, R.S., MacDonald, I.R., Fisher, C.R., . . . Burke Jr, R.A., 1990. Salt, seeps and symbiosis in the Gulf of Mexico. Eos, Transactions American Geophysical Union, 71(45): 1772-1773.

Brüning, M., Sahling, H., MacDonald, I.R., Ding, F., Bohrmann, G., 2010. Origin, distribution, and alteration of asphalts at Chapopote Knoll, Southern Gulf of Mexico. Marine and petroleum geology, 27(5): 1093-1106.

Bryant, W.R., Lugo, J., Córdova, C., Salvador, A., 1991. Physiography and bathymetry. The Gulf of Mexico Basin: Boulder, Geological Society of America, Decade of North American Geology, v. J: 13-30.

Burton, E.A., 1993. Controls on marine carbonate cement mineralogy: review and reassessment. Chemical Geology, 105(1-3): 163-179.

Burton, E.A., Walter, L.M., 1990. The role of pH in phosphate inhibition of calcite and aragonite precipitation rates in seawater. Geochimica et Cosmochimica Acta, 54(3): 797-808.

Butler, I.B., Böttcher, M.E., Rickard, D., Oldroyd, A., 2004. Sulfur isotope partitioning during experimental formation of pyrite via the polysulfide and hydrogen sulfide pathways: implications for the interpretation of sedimentary and hydrothermal pyrite isotope records. Earth and Planetary Science Letters, 228(3): 495-509.

Campbell, K.A., 2006. Hydrocarbon seep and hydrothermal vent paleoenvironments and paleontology: past developments and future research directions. Palaeogeography, Palaeoclimatology, Palaeoecology, 232(2): 362-407.

Campbell, K.A., Francis, D.A., Collins, M., Gregory, M.R., Nelson, C.S., Greinert, J., Aharon, P., 2008. Hydrocarbon seep-carbonates of a Miocene forearc (East Coast Basin), North Island, New Zealand. Sedimentary Geology, 204(3): 83-105.

Canet, C., Prol-Ledesma, R.M., Escobar-Briones, E., Mortera-Gutiérrez, C., Lozano-Santa Cruz, R., Linares, C., . . . Morales-Puente, P., 2006. Mineralogical and geochemical characterization of hydrocarbon seep sediments from the Gulf of Mexico. Marine and Petroleum Geology, 23(5): 605-619.

Canfield, D., 2001. Biogeochemistry of sulfur isotopes. Reviews in Mineralogy and Geochemistry, 43(1): 607-636.

Canfield, D.E., Kump, L.R., 2013. Carbon cycle makeover. Science, 339(6119): 533-534.

Canfield, D.E., Raiswell, R., Westrich, J.T., Reaves, C.M., Berner, R.A., 1986. The use of chromium reduction in the analysis of reduced inorganic sulfur in sediments and shales. Chemical geology, 54(1-2): 149-155.

Canfield, D.E., Thamdrup, B., 1994. The production of 34S-depleted sulfide during bacterial disproportionation of elemental sulfur. Science, 266(5193): 1973.

Cavagna, S., Clari, P., Martire, L., 1999. The role of bacteria in the formation of cold seep carbonates: geological evidence from Monferrato (Tertiary, NW Italy). Sedimentary Geology, 126(1): 253-270.

Chakraborty, A., Ruff, S.E., Dong, X., Ellefson, E.D., Li, C., Brooks, J.M., . . . Hubert, C.R.J., 2020. Hydrocarbon seepage in the deep seabed links subsurface and seafloor biospheres. Proceedings of the National Academy of Sciences, 117(20): 11029.

Chanton, J.P., 1985. Sulfur Mass Balance and Isotopic Fractionation in an Anoxic Marine Sediment. Ph.D. dissertation, University of North Carolina, Chapel Hill, North Carolina, 406 pp.

Chen, F., Wang, X., Li, N., Cao, J., Bayon, G., Peckmann, J., . . . Edwards, R.L., 2019. Gas hydrate dissociation during sea-level highstand inferred from U/Th dating of seep carbonate from the South China Sea. Geophysical Research Letters, 46(23): 13928-13938.

Cheng, H., Edwards, R.L., Shen, C.-C., Polyak, V.J., Asmerom, Y., Woodhead, J., . . . Spötl, C., 2013. Improvements in 230Th dating, 230Th and 234U half-life values, and U–Th isotopic

measurements by multi-collector inductively coupled plasma mass spectrometry. Earth and Planetary Science Letters, 371: 82-91.

Coffin, R.B., Osburn, C.L., Plummer, R.E., Smith, J.P., Rose, P.S., Grabowski, K.S., 2015. Deep sediment-sourced methane contribution to shallow sediment organic carbon: atwater valley, texas-louisiana shelf, gulf of mexico. Energies, 8(3): 1561-1583.

Colangelo-Lillis, J., Pelikan, C., Herbold, C.W., Altshuler, I., Loy, A., Whyte, L.G., Wing, B.A., 2019. Diversity decoupled from sulfur isotope fractionation in a sulfate-reducing microbial community. Geobiology, 17(6): 660-675.

Council, N.R., 2003. Oil in the sea III: inputs, fates, and effects. National Academies Press (US).

Crémière, A., Lepland, A., Chand, S., Sahy, D., Condon, D.J., Noble, S.R., . . . Brunstad, H., 2016. Timescales of methane seepage on the Norwegian margin following collapse of the Scandinavian Ice Sheet. Nature communications, 7.

Crémière, A., Pellerin, A., Wing, B.A., Lepland, A., 2020. Multiple sulfur isotopes in methane seep carbonates track unsteady sulfur cycling during anaerobic methane oxidation. Earth and Planetary Science Letters, 532: 115994.

Cui, H., Kaufman, A.J., Xiao, S., Zhou, C., Liu, X.-M., 2017. Was the Ediacaran Shuram Excursion a globally synchronized early diagenetic event? Insights from methane-derived authigenic carbonates in the uppermost Doushantuo Formation, South China. Chemical Geology, 450: 59-80.

D'souza, N., Subramaniam, A., Juhl, A.R., Hafez, M., Chekalyuk, A., Phan, S., . . . Montoya, J., 2016. Elevated surface chlorophyll associated with natural oil seeps in the Gulf of Mexico. Nature Geoscience.

Davidson, D.W., Leaist, D.G., Hesse, R., 1983. Oxygen-18 enrichment in the water of a clathrate hydrate. Geochimica et Cosmochimica Acta, 47(12): 2293-2295.

Davis Barnes, B., Husson, J.M., Peters, S.E., 2019. Authigenic Carbonate Burial in the Late Devonian–Early Mississippian Bakken Formation (Williston Basin, USA). Sedimentology.

Derry, L., 2014. Organic carbon cycling and the lithosphere.

Detmers, J., Brüchert, V., Habicht, K.S., Kuever, J., 2001. Diversity of sulfur isotope fractionations by sulfate-reducing prokaryotes. Applied and Environmental Microbiology, 67(2): 888-894.

Deusner, C., Holler, T., Arnold, G.L., Bernasconi, S.M., Formolo, M.J., Brunner, B., 2014. Sulfur and oxygen isotope fractionation during sulfate reduction coupled to anaerobic oxidation of methane is dependent on methane concentration. Earth and Planetary Science Letters, 399: 61-73.

Ding, F., Spiess, V., Brüning, M., Fekete, N., Keil, H., Bohrmann, G., 2008. A conceptual model for hydrocarbon accumulation and seepage processes around Chapopote asphalt site, southern Gulf of Mexico: from high resolution seismic point of view. Journal of Geophysical Research: Solid Earth, 113(B8).

Ding, F., Spiess, V., MacDonald, I.R., Brüning, M., Fekete, N., Bohrmann, G., 2010. Shallow sediment deformation styles in north-western Campeche Knolls, Gulf of Mexico and their controls on the occurrence of hydrocarbon seepage. Marine and petroleum geology, 27(4): 959-972.

Edwards, R.L., Chen, J., Wasserburg, G., 1987. 238U234U230Th232Th systematics and the precise measurement of time over the past 500,000 years. Earth and Planetary Science Letters, 81(2-3): 175-192.

Escobar-Briones, E., García-Villalobos, F.J., 2009. Distribution of total organic carbon and total nitrogen in deep-sea sediments from the southwestern Gulf of Mexico. Boletín de la Sociedad Geológica Mexicana, 61(1): 73-86.

Falkowski, P., Scholes, R., Boyle, E., Canadell, J., Canfield, D., Elser, J., . . . Linder, S., 2000. The global carbon cycle: a test of our knowledge of earth as a system. science, 290(5490): 291-296.

Fan, L.-F., Lin, S., Hsu, C.-W., Tseng, Y.-T., Yang, T.F., Huang, K.-M., 2018. Formation and preservation of authigenic pyrite in the methane dominated environment. Deep Sea Research Part I: Oceanographic Research Papers, 138: 60-71.

Feng, D., Chen, D., Roberts, H.H., 2009. Petrographic and geochemical characterization of seep carbonate from Bush Hill (GC 185) gas vent and hydrate site of the Gulf of Mexico. Marine and Petroleum Geology, 26(7): 1190-1198.

Feng, D., Peng, Y., Bao, H., Peckmann, J., Roberts, H.H., Chen, D., 2016. A carbonate-based proxy for sulfate-driven anaerobic oxidation of methane. Geology: G38233. 1.

Feng, D., Roberts, H.H., Cheng, H., Peckmann, J., Bohrmann, G., Edwards, R.L., Chen, D., 2010. U/Th dating of cold-seep carbonates: an initial comparison. Deep Sea Research Part II: Topical Studies in Oceanography, 57(21-23): 2055-2060.

Fike, D.A., Bradley, A.S., Rose, C.V., 2015. Rethinking the Ancient Sulfur Cycle. Annual Review of Earth and Planetary Sciences, 43(1): 593-622.

Fisher, C., Roberts, H., Cordes, E., Bernard, B., 2007. Cold seeps and associated communities of the Gulf of Mexico. Oceanography, 20(4): 118-129.

Flügel, E., 2004. Microfacies of carbonate rocks: analysis, interpretation and application. Springer.

Formolo, M.J., Lyons, T.W., 2013. Sulfur biogeochemistry of cold seeps in the Green Canyon region of the Gulf of Mexico. Geochimica et Cosmochimica Acta, 112: 264-285.

Formolo, M.J., Lyons, T.W., Zhang, C., Kelley, C., Sassen, R., Horita, J., Cole, D.R., 2004. Quantifying carbon sources in the formation of authigenic carbonates at gas hydrate sites in the Gulf of Mexico. Chemical Geology, 205(3): 253-264.

Gallagher, K.L., Kading, T.J., Braissant, O., Dupraz, C., Visscher, P.T., 2012. Inside the alkalinity engine: the role of electron donors in the organon ine.alization potential of sulfate-reducing bacteria. Geobiology, 10(6): 518-30.

Garrison, L.E., Martin, R.G., 1973. Geologic structures in the Gulf of Mexico basin, Geological Survey Professional Paper 773, U.S. Government Printing Office, Washington, D.C.

Gilhooly, W.P., Reinhard, C.T., Lyons, T.W., 2016. A comprehensive sulfur and oxygen isotope study of sulfur cycling in a shallow, hyper-euxinic meromictic lake. Geochimica et Cosmochimica Acta, 189: 1-23.

Gong, S., Peng, Y., Bao, H., Feng, D., Cao, X., Crockford, P.W., Chen, D., 2018. Triple sulfur isotope relationships during sulfate-driven anaerobic oxidation of methane. Earth and Planetary Science Letters, 504: 13-20.

Goñi, M.A., Ruttenberg, K.C., Eglinton, T.I., 1998. A reassessment of the sources and importance of land-derived organic matter in surface sediments from the Gulf of Mexico. Geochimica et Cosmochimica Acta, 62(18): 3055-3075.

Greinert, J., Bohrmann, G., Suess, E., 2001. Gas hydrate-associated carbonates and methane-venting at Hydrate Ridge: classification, distribution, and origin of authigenic lithologies. Natural gas hydrates: Occurrence, distribution, and detection: 99-113.

Habicht, K.S., Canfield, D.E., 1997. Sulfur isotope fractionation during bacterial sulfate reduction in organic-rich sediments. Geochimica et Cosmochimica Acta, 61(24): 5351-5361.

Habicht, K.S., Canfield, D.E., 2001. Isotope fractionation by sulfate-reducing natural populations and the isotopic composition of sulfide in marine sediments. Geology, 29(6): 555-558.

Havig, J.R., Hamilton, T.L., Bachan, A., Kump, L.R., 2017. Sulfur and carbon isotopic evidence for metabolic pathway evolution and a four-stepped Earth system progression across the Archean and Paleoproterozoic. Earth-Science Reviews, 174: 1-21.

Hayes, J.M., Strauss, H., Kaufman, A.J., 1999. The abundance of 13C in marine organic matter and isotopic fractionation in the global biogeochemical cycle of carbon during the past 800 Ma. Chemical Geology, 161(1-3): 103-125.

Higgins, J.A., Fischer, W., Schrag, D., 2009. Oxygenation of the ocean and sediments: consequences for the seafloor carbonate factory. Earth and Planetary Science Letters, 284(1-2): 25-33.

Himmler, T., Sahy, D., Martma, T., Bohrmann, G., Plaza-Faverola, A., Bünz, S., . . . Lepland, A., 2019. A 160,000-year-old history of tectonically controlled methane seepage in the Arctic. Science advances, 5(8): eaaw1450.

Hornafius, J.S., Quigley, D., Luyendyk, B.P., 1999. The world's most spectacular marine hydrocarbon seeps (Coal Oil Point, Santa Barbara Channel, California): Quantification of emissions. Journal of Geophysical Research: Oceans, 104(C9): 20703-20711.

Hovland, M., Jensen, S., Fichler, C., 2012. Methane and minor oil macro-seep systems—their complexity and environmental significance. Marine Geology, 332: 163-173.

Hovland, M., Talbot, M.R., Qvale, H., Olaussen, S., Aasberg, L., 1987. Methane-related carbonate cements in pockmarks of the North Sea. Journal of Sedimentary Research, 57(5): 881-892.

Jaffey, A., Flynn, K., Glendenin, L., Bentley, W.t., Essling, A., 1971. Precision measurement of half-lives and specific activities of U 235 and U 238. Physical review C, 4(5): 1889.

Jiang, G., Kennedy, M.J., Christie-Blick, N., 2003. Stable isotopic evidence for methane seeps in Neoproterozoic postglacial cap carbonates. Nature, 426(6968): 822-826.

Jiang, K., Zhang, J., Sakatoku, A., Kambayashi, S., Yamanaka, T., Kanehara, T., . . . Pellizari, V.H., 2018. Discovery and biogeochemistry of asphalt seeps in the North São Paulo Plateau, Brazilian Margin. Scientific reports, 8(1): 12619.

Jiang, L., Planavsky, N., Zhao, M., Liu, W., Wang, X., 2019. Authigenic origin for a massive negative carbon isotope excursion. Geology, 47(2): 115-118.

Jones, D.O., Walls, A., Clare, M., Fiske, M.S., Weiland, R.J., O'Brien, R., Touzel, D.F., 2014. Asphalt mounds and associated biota on the Angolan margin. Deep Sea Research Part I: Oceanographic Research Papers, 94: 124-136.

Jorgensen, B.B., 1979. A theoretical model of the stable sulfur isotope distribution in marine sediments. Geochimica et Cosmochimica Acta, 43(3): 363-374.

Jørgensen, B.B., Böttcher, M.E., Lüschen, H., Neretin, L.N., Volkov, I.I., 2004. Anaerobic methane oxidation and a deep H 2 S sink generate isotopically heavy sulfides in Black Sea sediments. Geochimica et Cosmochimica Acta, 68(9): 2095-2118.

Jørgensen, B.B., Findlay, A.J., Pellerin, A., 2019. The Biogeochemical Sulfur Cycle of Marine Sediments. Frontiers in Microbiology, 10(849).

Joye, S.B., Boetius, A., Orcutt, B.N., Montoya, J.P., Schulz, H.N., Erickson, M.J., Lugo, S.K., 2004. The anaerobic oxidation of methane and sulfate reduction in sediments from Gulf of Mexico cold seeps. Chemical Geology, 205(3): 219-238.

Judd, A., Hovland, M., 2009. Seabed fluid flow: the impact on geology, biology and the marine environment. Cambridge University Press.

Judd, A., Noble-James, T., Golding, N., Eggett, A., Diesing, M., Clare, D., . . . Milodowski, A., 2019. The Croker Carbonate Slabs: extensive methane-derived authigenic carbonate in the Irish Sea—nature, origin, longevity and environmental significance. Geo-Marine Letters: 1-16.

Kaplan, I.R., Rittenberg, S.C., 1964. Microbiological Fractionation of Sulphur Isotopes. Microbiology, 34(2): 195-212.

Katz, M.E., Wright, J.D., Miller, K.G., Cramer, B.S., Fennel, K., Falkowski, P.G., 2005. Biological overprint of the geological carbon cycle. Marine Geology, 217(3-4): 323-338.

Kemp, A.L.W., Thode, H.G., 1968. The mechanism of the bacterial reduction of sulphate and of sulphite from isotope fractionation studies. Geochimica et Cosmochimica Acta, 32(1): 71-91.

Kennedy, M.J., Christie-Blick, N., Sohl, L.E., 2001. Are Proterozoic cap carbonates and isotopic excursions a record of gas hydrate destabilization following Earth's coldest intervals? Geology, 29(5): 443-446.

Kennicutt, M.C., 2017. Oil and Gas Seeps in the Gulf of Mexico, Habitats and Biota of the Gulf of Mexico: Before the Deepwater Horizon Oil Spill. Springer, pp. 275-358.

Kiel, S., Peckmann, J., 2019. Resource partitioning among brachiopods and bivalves at ancient hydrocarbon seeps: A hypothesis. PLOS ONE, 14(9): e0221887.

Kim, S.-T., O'Neil, J.R., Hillaire-Marcel, C., Mucci, A., 2007. Oxygen isotope fractionation between synthetic aragonite and water: influence of temperature and Mg 2+ concentration. Geochimica et Cosmochimica Acta, 71(19): 4704-4715.

Klapp, S.A., Bohrmann, G., Kuhs, W.F., Murshed, M.M., Pape, T., Klein, H., . . . Abegg, F., 2010. Microstructures of structure I and II gas hydrates from the Gulf of Mexico. Marine and Petroleum Geology, 27(1): 116-125.

Kniemeyer, O., Musat, F., Sievert, S.M., Knittel, K., Wilkes, H., Blumenberg, M., . . . Joye, S.B., 2007. Anaerobic oxidation of short-chain hydrocarbons by marine sulphate-reducing bacteria. Nature, 449(7164): 898.

Körber, J.-H., Sahling, H., Pape, T., dos Santos Ferreira, C., MacDonald, I., Bohrmann, G., 2014. Natural oil seepage at kobuleti ridge, eastern Black Sea. Marine and Petroleum Geology, 50: 68-82.

Kump, L.R., 2012. SULFUR ISOTOPES AND THE STEPWISE OXYGENATION OF THE BIOSPHERE. Elements, 8(6): 410-411.

Kump, L.R., Arthur, M.A., 1999. Interpreting carbon-isotope excursions: carbonates and organic matter. Chemical Geology, 161(1-3): 181-198.

Kvenvolden, K., Cooper, C., 2003. Natural seepage of crude oil into the marine environment. Geo-Marine Letters, 23(3-4): 140-146.

Kvenvolden, K.A., Harbaugh, J.W., 1983. Reassessment of the rates at which oil from natural sources enters the marine environment. Marine Environmental Research, 10(4): 223-243.

Laso-Pérez, R., Hahn, C., van Vliet, D.M., Tegetmeyer, H.E., Schubotz, F., Smit, N.T., . . . Boetius, A., 2019. Anaerobic Degradation of Non-Methane Alkanes by "Candidatus Methanoliparia" in Hydrocarbon Seeps of the Gulf of Mexico. mBio, 10(4): e01814-19.

Leavitt, W.D., Halevy, I., Bradley, A.S., Johnston, D.T., 2013. Influence of sulfate reduction rates on the Phanerozoic sulfur isotope record. Proceedings of the National Academy of Sciences, 110(28): 11244.

Li, N., Feng, D., Chen, L., Wang, H., Chen, D., 2016. Using sediment geochemistry to infer temporal variation of methane flux at a cold seep in the South China Sea. Marine and Petroleum Geology, 77: 835-845.

Li, N., Yang, X., Peng, J., Zhou, Q., Chen, D., 2017. Paleo-cold seep activity in the southern South China Sea: Evidence from the geochemical and geophysical records of sediments. Journal of Asian Earth Sciences.

Liebetrau, V., Eisenhauer, A., Linke, P., 2010. Cold seep carbonates and associated cold-water corals at the Hikurangi Margin, New Zealand: new insights into fluid pathways, growth structures and geochronology. Marine Geology, 272(1): 307-318.

Lim, Y.C., Lin, S., Yang, T.F., Chen, Y.-G., Liu, C.-S., 2011. Variations of methane induced pyrite formation in the accretionary wedge sediments offshore southwestern Taiwan. Marine and Petroleum Geology, 28(10): 1829-1837.

Lin, Q., Wang, J., Taladay, K., Lu, H., Hu, G., Sun, F., Lin, R., 2016a. Coupled pyrite concentration and sulfur isotopic insight into the paleo sulfate–methane transition zone (SMTZ) in the northern South China Sea. Journal of Asian Earth Sciences, 115: 547-556.

Lin, Z., Sun, X., Lu, Y., Strauss, H., Xu, L., Gong, J., . . . Sun, W., 2017a. The enrichment of heavy iron isotopes in authigenic pyrite as a possible indicator of sulfate-driven anaerobic oxidation of methane: Insights from the South China Sea. Chemical Geology, 449: 15-29.

Lin, Z., Sun, X., Peckmann, J., Lu, Y., Xu, L., Strauss, H., . . . Teichert, B.M., 2016b. How sulfate-driven anaerobic oxidation of methane affects the sulfur isotopic composition of pyrite: a SIMS study from the South China Sea. Chemical Geology, 440: 26-41.

Lin, Z., Sun, X., Strauss, H., Lu, Y., Böttcher, M.E., Teichert, B.M.A., . . . Peckmann, J., 2018. Multiple sulfur isotopic evidence for the origin of elemental sulfur in an iron-dominated gas hydrate-bearing sedimentary environment. Marine Geology, 403: 271-284.

Lin, Z., Sun, X., Strauss, H., Lu, Y., Gong, J., Xu, L., . . . Peckmann, J., 2017b. Multiple sulfur isotope constraints on sulfate-driven anaerobic oxidation of methane: Evidence from authigenic pyrite in seepage areas of the South China Sea. Geochimica et Cosmochimica Acta, 211: 153-173.

Liu, J., Pellerin, A., Izon, G., Wang, J., Antler, G., Liang, J., . . . Ono, S., 2020. The multiple sulphur isotope fingerprint of a sub-seafloor oxidative sulphur cycle driven by iron. Earth and Planetary Science Letters, 536: 116165.

Lu, Y., Sun, X., Xu, H., Konishi, H., Lin, Z., Xu, L., . . . Peckmann, J., 2018. Formation of dolomite catalyzed by sulfate-driven anaerobic oxidation of methane: Mineralogical and geochemical evidence from the northern South China Sea. American Mineralogist, 103(5): 720-734.

Lyons, T., Gill, B., 2010. Ancient Sulfur Cycling and Oxygenation of the Early Biosphere. Elements, 6: 93-99.

Lyons, T.W., 1992. Contrasting sediment types from oxic and anoxic sites of the modern Black Sea: Geochemical and sedimentological criteria. Ph.D. Thesis, Yale University, Ann Arbor, 396 pp.

Lyons, T.W., 1997. Sulfur isotopic trends and pathways of iron sulfide formation in upper Holocene sediments of the anoxic Black Sea. Geochimica et Cosmochimica Acta, 61(16): 3367-3382.

Lyons, T.W., Reinhard, C.T., Planavsky, N.J., 2014. The rise of oxygen in Earth's early ocean and atmosphere. Nature, 506(7488): 307-315.

Lyons, T.W., Walter, L.M., Gellatly, A.M., Martini, A.M., Blake, R.E., 2004. Sites of anomalous organic remineralization in the carbonate sediments of South Florida, USA: the sulfur cycle and carbonate-associated sulfate. Geological Society of America Special Papers, 379: 161-176.

MacDonald, I., Bohrmann, G., Escobar, E., Abegg, F., Blanchon, P., Blinova, V., . . . Han, X., 2004. Asphalt volcanism and chemosynthetic life in the Campeche Knolls, Gulf of Mexico. Science, 304(5673): 999-1002.

MacDonald, I.R., Garcia-Pineda, O., Beet, A., Daneshgar Asl, S., Feng, L., Graettinger, G., . . . Huffer, F., 2015. Natural and unnatural oil slicks in the Gulf of Mexico. Journal of Geophysical Research: Oceans, 120(12): 8364-8380.

Mansour, A.S., 2014. Hydrocarbon-derived carbonates along the upper–lower continental slope, Gulf of Mexico: a mineralogical and stable isotopic study. Carbonates and Evaporites, 29(1): 89-105.

Mansour, A.S., Sassen, R., 2011. Mineralogical and stable isotopic characterization of authigenic carbonate from a hydrocarbon seep site, Gulf of Mexico slope: possible relation to crude oil degradation. Marine Geology, 281(1-4): 59-69.

Marcon, Y., Sahling, H., MacDonald, I.R., Wintersteller, P., dos Santos Ferreira, C., Bohrmann, G., 2018. Slow volcanoes: the intriguing similarities between marine asphalt and basalt lavas. Oceanography, 31(2): 194-205.

Marlow, J., Peckmann, J., Orphan, V., 2015. Autoendoliths: a distinct type of rock-hosted microbial life. Geobiology, 13(4): 303-307.

Marlow, J.J., Steele, J.A., Ziebis, W., Thurber, A.R., Levin, L.A., Orphan, V.J., 2014. Carbonate-hosted methanotrophy represents an unrecognized methane sink in the deep sea. Nature communications, 5.

Mazumdar, A., Dewangan, P., Joäo, H., Peketi, A., Khosla, V., Kocherla, M., . . . Ramamurty, P., 2009. Evidence of paleo–cold seep activity from the Bay of Bengal, offshore India. Geochemistry, Geophysics, Geosystems, 10(6).

Mazzini, A., Svensen, H.H., Forsberg, C.F., Linge, H., Lauritzen, S.-E., Haflidason, H., . . . Tjelta, T.I., 2017. A climatic trigger for the giant Troll pockmark field in the northern North Sea. Earth and Planetary Science Letters, 464: 24-34.

McQueen, J., 1967. Some methods for classification and analysis of multivariate observations. Computer and Chemistry, 4: 257-272.

Meister, P., 2013. Two opposing effects of sulfate reduction on carbonate precipitation in normal marine, hypersaline, and alkaline environments. Geology, 41(4): 499-502.

Meister, P., Liu, B., Khalili, A., Böttcher, M.E., Jørgensen, B.B., 2019. Factors controlling the carbon isotope composition of dissolved inorganic carbon and methane in marine porewater: An evaluation by reaction-transport modelling. Journal of Marine Systems, 200: 103227.

Mitchell, R., MacDonald, I., Kvenvolden, K., 1999. Estimates of total hydrocarbon seepage into the Gulf of Mexico based on satellite remote sensing images. EOS Supplement, 80(49): OS242.

Naehr, T., Rodriguez, N., Bohrmann, G., Paull, C., Botz, R., 2000. 29. Methanederived authigenic carbonates associated with gas hydrate decomposition and fluid venting above the Blake Ridge Diapir, Proceedings of the Ocean Drilling Program, Scientific Results, pp. 285-300.

Naehr, T.H., Birgel, D., Bohrmann, G., MacDonald, I.R., Kasten, S., 2009. Biogeochemical controls on authigenic carbonate formation at the Chapopote "asphalt volcano", Bay of Campeche. Chemical Geology, 266(3): 390-402.

Naehr, T.H., Eichhubl, P., Orphan, V.J., Hovland, M., Paull, C.K., Ussler Iii, W., . . . Greene, H.G., 2007. Authigenic carbonate formation at hydrocarbon seeps in continental margin sediments: A comparative study. Deep Sea Research Part II: Topical Studies in Oceanography, 54(11-13): 1268-1291.

Noble, R., Orange, D., Decker, J., Teas, P., Baillie, P., 2009. Oil and gas seeps in deep marine sea floor cores as indicators of active petroleum systems in Indonesia, 33rd annual convention, Indonesian Petroleum Association, Jakarta, pp. 385-394.

Oppo, D., De Siena, L., Kemp, D.B., 2020. A record of seafloor methane seepage across the last 150 million years. Scientific Reports, 10(1): 2562.

Orcutt, B.N., Joye, S.B., Kleindienst, S., Knittel, K., Ramette, A., Reitz, A., . . . Boetius, A., 2010. Impact of natural oil and higher hydrocarbons on microbial diversity, distribution, and activity in Gulf of Mexico cold-seep sediments. Deep Sea Research Part II: Topical Studies in Oceanography, 57(21-23): 2008-2021.

Pancost, R.D., Zhang, C.L., Tavagoli, J., Talbot, H.M., Farrimond, P., Schouten, S., . . . Sassen, R., 2005. Lipid biomarkers preserved in hydrate-associated authigenic carbonate rocks of the Gulf of Mexico. Palaeogeography, Palaeoclimatology, Palaeoecology, 227(1): 48-66.

Peckmann, J., Campbell, K.A., Walliser, O.H., Reitner, J., 2007. A Late Devonian Hydrocarbon-Seep Deposit Dominated by Dimerelloid Brachiopods, Morocco. PALAIOS, 22(2): 114-122.

Peckmann, J., Goedert, J., Thiel, V., Michaelis, W., Reitner, J., 2002. A comprehensive approach to the study of methane-seep deposits from the Lincoln Creek Formation, western Washington State, USA. Sedimentology, 49(4): 855-873.

Peckmann, J., Reimer, A., Luth, U., Luth, C., Hansen, B., Heinicke, C., . . . Reitner, J., 2001. Methane-derived carbonates and authigenic pyrite from the northwestern Black Sea. Marine geology, 177(1-2): 129-150.

Peckmann, J., Thiel, V., 2004. Carbon cycling at ancient methane–seeps. Chemical Geology, 205(3): 443-467.

Peketi, A., Mazumdar, A., Joao, H., Patil, D., Usapkar, A., Dewangan, P., 2015. Coupled C–S–Fe geochemistry in a rapidly accumulating marine sedimentary system: Diagenetic and depositional implications. Geochemistry, Geophysics, Geosystems, 16(9): 2865-2883.

Peketi, A., Mazumdar, A., Joshi, R., Patil, D., Srinivas, P., Dayal, A., 2012. Tracing the Paleo sulfate-methane transition zones and H2S seepage events in marine sediments: An application of C-S-Mo systematics. Geochemistry, Geophysics, Geosystems, 13(10).

Pellerin, A., Antler, G., Holm, S.A., Findlay, A.J., Crockford, P.W., Turchyn, A.V., . . . Finster, K., 2019. Large sulfur isotope fractionation by bacterial sulfide oxidation. Science Advances, 5(7): eaaw1480.

Price, F.T., Shieh, Y., 1979. Fractionation of sulfur isotopes during laboratory synthesis of pyrite at low temperatures. Chemical Geology, 27(3): 245-253.

Prouty, N.G., Sahy, D., Ruppel, C.D., Roark, E.B., Condon, D., Brooke, S., . . . Demopoulos, A.W., 2016. Insights into methane dynamics from analysis of authigenic carbonates and chemosynthetic mussels at newly-discovered Atlantic Margin seeps. Earth and Planetary Science Letters, 449: 332-344.

Raiswell, R., 1987. Non-steady state microbiological diagenesis and the origin of concretions and nodular limestones. Geological Society, London, Special Publications, 36(1): 41-54.

Rickard, D., Mussmann, M., Steadman, J.A., 2017. Sedimentary Sulfides. Elements, 13(2): 117-122.

Ritger, S., Carson, B., Suess, E., 1987. Methane-derived authigenic carbonates formed by subduction-induced pore-water expulsion along the Oregon/Washington margin. Geological Society of America Bulletin, 98(2): 147-156.

Roberts, H.H., 2001. Fluid and Gas Expulsion on the Northern Gulf of Mexico Continental Slope: Mud-Prone to Mineral-Prone Responses. Natural gas hydrates: occurrence, distribution, and detection: 145-161.

Roberts, H.H., Aharon, P., 1994. Hydrocarbon-derived carbonate buildups of the northern Gulf of Mexico continental slope: a review of submersible investigations. Geo-Marine Letters, 14(2-3): 135-148.

Roberts, H.H., Carney, R.S., 1997. Evidence of episodic fluid, gas, and sediment venting on the northern Gulf of Mexico continental slope. Economic Geology, 92(7-8): 863-879.

Roberts, H.H., Feng, D., 2013. Carbonate Precipitation at Gulf of Mexico Hydrocarbon Seeps: An Overview, Hydrocarbon Seepage: From Source to Surface. SEG and AAPG, pp. 43-61.

Roberts, H.H., Feng, D., Joye, S.B., 2010. Cold seep carbonates of the middle and lower continental slope, northern Gulf of Mexico. Deep sea research part II: Topical Studies in Oceanography, 57(21-23): 2040-2054.

Römer, M., Hsu, C.-W., Loher, M., MacDonald, I., dos Santos Ferreira, C., Pape, T., . . . Sahling, H., 2019. Amount and fate of gas and oil discharged at 3400 m water depth from a natural seep site in the Southern Gulf of Mexico. Frontiers in Marine Science, 6: 700.

Rowe, G.T., 2017. Offshore Plankton and Benthos of the Gulf of Mexico. In: Ward, C.H. (Ed.), Habitats and Biota of the Gulf of Mexico: Before the Deepwater Horizon Oil Spill: Volume 1: Water Quality, Sediments, Sediment Contaminants, Oil and Gas Seeps, Coastal Habitats, Offshore Plankton and Benthos, and Shellfish. Springer New York, New York, NY, pp. 641-767.

Sahling, H., Borowski, C., Escobar-Briones, E., Gaytán-Caballero, A., Hsu, C.-W., Loher, M., . . . Römer, M., 2016. Massive asphalt deposits, oil seepage, and gas venting support abundant chemosynthetic communities at the Campeche Knolls, southern Gulf of Mexico. Biogeosciences, 13(15): 4491-4512.

Salas-de-León, D.A., Monreal-Gómez, M.A., Díaz-Flores, M.A., Salas-Monreal, D., Velasco-Mendoza, H., Riverón-Enzástiga, M.L., Ortiz-Zamora, G., 2008. Role of Near-Bottom Currents in the Distribution of Sediments within the Southern Bay of Campeche, Gulf of Mexico. Journal of Coastal Research, 24(6 (246)): 1487-1494.

Salvador, A., 1991. Origin and development of the Gulf of Mexico basin. The gulf of Mexico basin: 389-444.

Sassen, R., Brooks, J.M., MacDonald, I.R., Kennicutt II, M.C., Guinasso Jr, N.L., Requejo, A.G., 1993. Association of oil seeps and chemosynthetic communities with oil discoveries, upper continental slope, Gulf of Mexico.

Sassen, R., MacDonald, I.R., Guinasso, N.L., Joye, S., Requejo, A.G., Sweet, S.T., . . . Schink, D.R., 1998. Bacterial methane oxidation in sea-floor gas hydrate: significance to life in extreme environments. Geology, 26(9): 851-854.

Sassen, R., MacDonald, I.R., Requejo, A.G., Guinasso, N.L., Kennicutt, M.C., Sweet, S.T., Brooks, J.M., 1994. Organic geochemistry of sediments from chemosynthetic communities, Gulf of Mexico slope. Geo-Marine Letters, 14(2): 110-119.

Sassen, R., Roberts, H.H., Carney, R., Milkov, A.V., DeFreitas, D.A., Lanoil, B., Zhang, C., 2004. Free hydrocarbon gas, gas hydrate, and authigenic minerals in chemosynthetic communities of the northern Gulf of Mexico continental slope: relation to microbial processes. Chemical Geology, 205(3-4): 195-217.

Sassen, R., Sweet, S.T., DeFreitas, D.A., Morelos, J.A., Milkov, A.V., 2001. Gas hydrate and crude oil from the Mississippi Fan Foldbelt, downdip Gulf of Mexico Salt Basin: significance to petroleum system. Organic Geochemistry, 32(8): 999-1008.

Sauer, S., Crémière, A., Knies, J., Lepland, A., Sahy, D., Martma, T., . . . Schubert, C.J., 2017. U-Th chronology and formation controls of methane-derived authigenic carbonates from the Hola trough seep area, northern Norway. Chemical Geology, 470: 164-179.

Schrag, D.P., Higgins, J.A., Macdonald, F.A., Johnston, D.T., 2013. Authigenic carbonate and the history of the global carbon cycle. science, 339(6119): 540-543.

Schubotz, F., Lipp, J.S., Elvert, M., Hinrichs, K.-U., 2011a. Stable carbon isotopic compositions of intact polar lipids reveal complex carbon flow patterns among hydrocarbon degrading microbial communities at the Chapopote asphalt volcano. Geochimica et Cosmochimica Acta, 75(16): 4399-4415.

Schubotz, F., Lipp, J.S., Elvert, M., Kasten, S., Mollar, X.P., Zabel, M., . . . Hinrichs, K.-U., 2011b. Petroleum degradation and associated microbial signatures at the Chapopote asphalt volcano, Southern Gulf of Mexico. Geochimica et Cosmochimica Acta, 75(16): 4377-4398.

Shackleton, N.J., 1985. Oceanic carbon isotope constraints on oxygen and carbon dioxide in the Cenozoic atmosphere. The carbon cycle and atmospheric CO2: natural variations Archean to present, 32: 412-417.

Sim, M.S., Ono, S., Donovan, K., Templer, S.P., Bosak, T., 2011. Effect of electron donors on the fractionation of sulfur isotopes by a marine Desulfovibrio sp. Geochimica et Cosmochimica Acta, 75(15): 4244-4259.

Smrzka, D., Feng, D., Himmler, T., Zwicker, J., Hu, Y., Monien, P., . . . Peckmann, J., 2020. Trace elements in methane-seep carbonates: Potentials, limitations, and perspectives. Earth-Science Reviews, 208: 103263.

Smrzka, D., Zwicker, J., Klügel, A., Monien, P., Bach, W., Bohrmann, G., Peckmann, J., 2016. Establishing criteria to distinguish oil-seep from methane-seep carbonates. Geology, 44(8): 667-670.

Smrzka, D., Zwicker, J., Lu, Y., Sun, Y., Feng, D., Monien, P., . . . Peckmann, J., 2021. Trace element distribution in methane-seep carbonates: The role of mineralogy and dissolved sulfide. Chemical Geology: 120357.

Smrzka, D., Zwicker, J., Misch, D., Walkner, C., Gier, S., Monien, P., . . . Peckmann, J., 2019. Oil seepage and carbonate formation: A case study from the southern Gulf of Mexico. Sedimentology.

Suess, E., 2018. Marine Cold Seeps: Background and Recent Advances. Hydrocarbons, Oils and Lipids: Diversity, Origin, Chemistry and Fate: 1-21.

Sun, X., Turchyn, A.V., 2014. Significant contribution of authigenic carbonate to marine carbon burial. Nature Geoscience, 7(3): 201-204.

Sun, Y., Gong, S., Li, N., Peckmann, J., Jin, M., Roberts, H.H., . . . Feng, D., 2020. A new approach to discern the hydrocarbon sources (oil vs methane) of authigenic carbonates forming at marine seeps. Marine and Petroleum Geology: 104230.

Suresh, G., 2015. Offshore oil seepage visible from space: A Synthetic Aperture Radar (SAR) based automatic detection, mapping and quantification system, Universität Bremen.

Teichert, B., Eisenhauer, A., Bohrmann, G., Haase-Schramm, A., Bock, B., Linke, P., 2003. U/Th systematics and ages of authigenic carbonates from Hydrate Ridge, Cascadia Margin: recorders of fluid flow variations. Geochimica et Cosmochimica Acta, 67(20): 3845-3857.

Torres, M.E., Hong, W.-L., Solomon, E.A., Milliken, K., Kim, J.-H., Sample, J.C., . . . Wallmann, K., 2020. Silicate weathering in anoxic marine sediment as a requirement for authigenic carbonate burial. Earth-Science Reviews, 200: 102960.

Valentine, D.L., Reddy, C.M., Farwell, C., Hill, T.M., Pizarro, O., Yoerger, D.R., . . . Bagby, S.C., 2010. Asphalt volcanoes as a potential source of methane to late Pleistocene coastal waters. Nature Geoscience, 3(5): 345-348.

Wallmann, K., Aloisi, G., Haeckel, M., Tishchenko, P., Pavlova, G., Greinert, J., . . . Eisenhauer, A., 2008. Silicate weathering in anoxic marine sediments. Geochimica et Cosmochimica Acta, 72(12): 2895-2918.

Wang, J., Chen, Q., Wei, Q., Wang, X., Li, Q., Gao, Y., 2008. Authigenic pyrites and their stable sulfur isotopes in sediments from IODP 311 on Cascadia margin, northeastern pacific, 6th International Conference on Gas Hydrates, Vancouver.

Watanabe, Y., Nakai, S.i., Hiruta, A., Matsumoto, R., Yoshida, K., 2008. U–Th dating of carbonate nodules from methane seeps off Joetsu, Eastern Margin of Japan Sea. Earth and Planetary Science Letters, 272(1): 89-96.

Wehrmann, L.M., Templer, S.P., Brunner, B., Berrasconi, S.M., Maignien, L., Ferdelman, T.G., 2011. The imprint of methane seepage on the geochemical record and early diagenetic processes in cold-water coral mounds on Pen Duick Escarpment, Gulf of Cadiz. Marine Geology, 282(1): 118-137.

Wei, J., Wu, T., Zhang, W., Deng, Y., Xie, R., Peng, J., . . . Cao, J., 2020. Deeply Buried Authigenic Carbonates in the Qiongdongnan Basin, South China Sea: Implications for Ancient Cold Seep Activities. Minerals, 10(12)

Widdel, F., Rabus, R., 2001. Anaerobic biodegradation of saturated and aromatic hydrocarbons. Current opinion in biotechnology, 12(3): 259-276.

Wilson, R., Monaghan, P., Osanik, A., Price, L., Rogers, M., 1974. Natural marine oil seepage. Science, 184(4139): 857-865

Wirsig, C., Kowsmann, R.O., Miller, D.J., de Oliveira Godoy, J.M., Mangini, A., 2012. U/Th-dating and post-depositional alteration of a cold seep carbonate chimney from the Campos Basin offshore Brazil. Marine Geology, 329: 24-33.

Wu, D., Sun, T., Xie, R., Pan, M., Chen, X., Ye, Y., . . . Wu, N., 2019. Characteristics of Authigenic Minerals around the Sulfate-Methane Transition Zone in the Methane-Rich Sediments of the Northern South China Sea: Inorganic Geochemical Evidence. International journal of environmental research and public health, 16(13): 2299.

Yanagawa, K., Shiraishi, F., Tanigawa, Y., Maeda, T., Mustapha, N.A., Owari, S., . . . Kano, A., 2019. Endolithic microbial habitats hosted in carbonate nodules currently forming within sediment at a high methane flux site in the sea of Japan. Geosciences, 9(11): 463.

Zhang, F., Xu, H., Konishi, H., Kemp, J.M., Roden, E.E., Shen, Z., 2012. Dissolved sulfide-catalyzed precipitation of disordered dolomite: Implications for the formation mechanism of sedimentary dolomite. Geochimica et Cosmochimica Acta, 97: 148-165.

Zhang, F., Yan, C., Teng, H.H., Roden, E.E., Xu, H., 2013. In situ AFM observations of Ca–Mg carbonate crystallization catalyzed by dissolved sulfide: Implications for sedimentary dolomite formation. Geochimica et Cosmochimica Acta, 105: 44-55.

Zhang, S., 2020. The relationship between organoclastic sulfate reduction and carbonate precipitation/dissolution in marine sediments. Marine Geology, 428: 106284.

Zhao, M.-Y., Zheng, Y.-F., Zhao, Y.-Y., 2016. Seeking a geochemical identifier for authigenic carbonate. Nature communications, 7.

Highlights:

- We present new insights into the geological signatures of anaerobic crude oil oxidation coupled with sulfate reduction using authigenic carbonate geochemistry from southern Gulf of Mexico (Chapopote asphalt volcano, Bay of Campeche).
- We report the first U-Th-based ages for seep carbonates from southern Gulf of Mexico. U-Th age-dating of Chapopote seep carbonate samples yielded ages of 13.5 ka – 4.6 ka before present (BP), suggesting that Chapopote asphalt seepage has been ongoing for thousands of years.
- We report distinguishable variation in the paired $\delta^{13}C_{DIC}$ and $\delta^{34}S_{sulfide}$ signatures produced via sulfate-driven anaerobic oxidation of methane (AOM) and non-methane hydrocarbons AONM), which can be reconstructed through paired $\delta^{13}C_{CaCO3}$ and $\delta^{34}S_{sulfide\text{-}mineral}$ signals in seep carbonates.
- We present a $\delta^{13}C_{CaCO3}$ vs. $\delta^{34}S_{CRS}$ cross plot to distinguish and classify the near-surface authigenic carbonate systems in the Gulf of Mexico formed due to anaerobic methane oxidation and crude oil oxidation.